



저작자표시-비영리-변경금지 2.0 대한민국

이용자는 아래의 조건을 따르는 경우에 한하여 자유롭게

- 이 저작물을 복제, 배포, 전송, 전시, 공연 및 방송할 수 있습니다.

다음과 같은 조건을 따라야 합니다:



저작자표시. 귀하는 원저작자를 표시하여야 합니다.



비영리. 귀하는 이 저작물을 영리 목적으로 이용할 수 없습니다.



변경금지. 귀하는 이 저작물을 개작, 변형 또는 가공할 수 없습니다.

- 귀하는, 이 저작물의 재이용이나 배포의 경우, 이 저작물에 적용된 이용허락조건을 명확하게 나타내어야 합니다.
- 저작권자로부터 별도의 허가를 받으면 이러한 조건들은 적용되지 않습니다.

저작권법에 따른 이용자의 권리는 위의 내용에 의하여 영향을 받지 않습니다.

이것은 [이용허락규약\(Legal Code\)](#)을 이해하기 쉽게 요약한 것입니다.

[Disclaimer](#)

Dissertation for the degree of Doctor of Philosophy

**Laser-Generated Focused Ultrasound for  
Brain Stimulation Using Carbon Nanotube  
Composite Transducer**

**Jooho Lee**

Department of Faculty of Earth and Marine Convergence,  
Major of Ocean System  
The Graduate School  
Jeju National University

**February 2024**

# Laser-Generated Focused Ultrasound for Brain Stimulation Using Carbon Nanotube Composite Transducer

A Dissertation submitted to the graduate school of  
Jeju National University in partial fulfillment of  
the requirements for the degree of Doctor of Philosophy  
under the supervision of **Dong-Guk Paeng**

The dissertation for the degree of Doctor of Philosophy  
by **Jooho Lee**  
has been approved by the dissertation committee.

December 2023

Chair	Younjoung Kang_____
Member	Dong-Guk Paeng_____
Member	Jinhyoung Park_____
Member	Changsoo Kim_____
Member	Bokyeong Ryu_____

## CONTENTS

<b>CONTENTS</b> .....	<b>3</b>
<b>LIST OF FIGURES</b> .....	<b>7</b>
<b>LIST OF TABLES</b> .....	<b>14</b>
<b>ABSTRACT</b> .....	<b>15</b>
<b>CHAPTER I INTRODUCTION</b> .....	<b>17</b>
1.1 Background of Therapeutical Ultrasound.....	17
1.2 Neuromodulation Of Therapeutic Ultrasound.....	25
1.3 Characteristics of LGFUS.....	28
1.4 Motivation.....	30
1.5 Specific Aims.....	32
1.6 Thesis Outline.....	34
<b>CHAPTER II LASER GENERATED FOCUSED ULTRASOUND AND TRANSDUCER STRUCTURE</b> .....	<b>35</b>
2.1 Background.....	35
2.2 Principles of LGFUS.....	38
2.3 Materials and Method.....	43
2.3.1 Fabrication of CNT composite transducer.....	43
2.3.2 Difference structure of LGFUS transducer.....	45

2.3.3 LGFUS Acquisition .....	47
2.4 Results.....	49
2.4.1 Structure Changing of CNT Composite Transducer.....	49
2.4.2 Acoustic Pressure According to Diameter Changing.....	51
2.4.3 Relationship between Laser Energy and Acoustic Pressure.....	54
2.5 Discussion.....	60
2.6 Conclusion.....	64
<b>CHAPTER III APPLICATION OF LASER GENERATED FOCUSED ULTRASOUND .....</b>	<b>65</b>
3.1 Application of Rat using LGFUS.....	65
3.2 Method and Experimental Set up.....	67
3.2.1 Animal Preparation.....	67
3.2.2 EEG Signal Acquisition and Analysis.....	67
3.2.3 Experimental set up.....	69
3.2.4 LGFUS Acquisition.....	71
3.3 Results.....	73
3.3.1 EEG Channel Selection.....	73
3.3.2 EEG Real Time Monitoring during LGFUS Brain Stimulation.....	76

3.3.3 EEG Signal Before and After LGFUS Brain Stimulation.....	80
3.4 Discussion.....	88
3.5 Conclusion.....	94
<b>CHAPTER IV PRELIMINARY EXPERIMENT TO EXPLORE THE CHARACTERISTICS OF LGFUS THROUGH HUMAN SKULL CADAVER.....</b>	<b>95</b>
4.1 Introduction.....	95
4.2 Material and Experimental set up.....	98
4.2.1 Skull Acquisition.....	98
4.2.2 Morphological Information and Experimental Set up.....	98
4.3 Results.....	101
4.3.1 Characterization of LGFUS with and without Skull Cadaver.....	101
4.3.2 Comparison of HIFU and LGFUS with and without Skull Cadaver Penetration .....	104
4.4 Discussion.....	107
4.5 Conclusion.....	110
<b>CHAPTER V CONCLUSION AND FUTURE STUDIES.....</b>	<b>111</b>
5.1 Conclusion.....	111
5.2 Future Studies.....	113

**REFERENCE.....115**  
**ACKNOWLEDGEMENTS.....122**

## LIST OF FIGURES

- Figure 1.1 Historical development sequence and research trends of therapeutic ultrasound. ..19
- Figure 1.2 Types according to characteristics, mechanism, and application of therapeutic ultrasound. ....24
- Figure 2.1 The principle of LGFUS transducer and sequence of converting laser energy to shock wave for LGFUS. The CNT composite layer receives the thermal energy of the laser and generates a LGFUS through contraction and expansion. ....42
- Figure 2.2 (a) The fabrication process of LGFUS transducers. The CNT aqueous solution is spray-coated onto a concave acrylic substrate and dried at room temperature. PDMS is spin-coated onto the surface of the dried CNT layer at 2000 RPM for 2 minutes and dried at 100 ° C for 1 hour. (b) SEM image of LGFUS transducer structure. The green box is CNT-PDMS composite layer, and blue box is an acrylic substrate layer. ....44
- Figure 2.3 The shape of the LGFUS transducer about the backing structure of the transducer substrate and changes in substrate diameter. (a) 20 mm diameter transducer substrate base design that converts acrylic-backing to air and water-backing using a 14 mm hole at the center of the substrate. (b) CNT-PDMS composite transducers of different sizes were used in the experiment. The top view of 8 cm, 5 cm, and 2 cm transducers, along with their side view, are presented. ....46

Figure 2.4 Experimental setup for LGFUS generation and measurement. The CNT-PDMS composite transducer was mounted inside a degassed water tank and aligned with the laser system (Q-switched Nd: YAG laser (STL-5000Q, Stratek, Anyang-si, Korea). The needle hydrophone (NH0200, Precision Acoustics Ltd., Dorchester, UK) collected the LGFUS signal generated from the CNTPDMS composite transducer, which was then amplified by a pre-amplifier (HP Precision Acoustics. Ltd., Dorchester, UK) and sent to the oscilloscope (LT354, Lecroy, New York, NY, USA). The signal data from the oscilloscope were fed to a PC for analysis .....48

Figure 2.5 Acoustic pressure from CNT composite transducer with laser energy for different backing layer. (a) LGFUS signal generated from the CNT composite transducer supported by acrylic, water, and air when the laser energy of 700 mJ. (b) The positive and negative pressures according to laser energy about all three transducer backing structures. .... 50

Figure 2.6 Waveforms and their spectra of measured pressure showing the peak positive and negative pressures of the LGFUS generated by CNT composite transducers of different diameters. Figures (a–c) show the time domain signals, while (d–f) shows the frequency domain analysis of the 2 cm, 5 cm, and 8 cm CNT composite transducers, respectively. ....52

Figure 2.7 Linear curve fitting shows the relationship between laser energy and the acoustic pressure generated by CNT-PDMS composite transducers. It shows a linear relationship between laser energy and positive and negative acoustic pressures in all transducers, except the transducer with a 2 cm diameter. It shows saturation at -10 MPa in negative pressure with increased laser energy. ....55

Figure 2.8 Scatter graph of predicted and experimental (measured) data of the CNT composite transducer for different diameters. The black circle and blue triangle marks correspond to the predicted values, while the green and pink star marks represent the measured values. This prediction was made at the laser energy of 700 mJ/pulse, and 800 mJ/pulse. ....58

Figure 2.9 (a) CNT composite transducer of 2cm diameter. (b) LGFUS according to laser energy from CNT composite transducer of 2 cm diameter. (c) Experimental setup for measuring the focal point of the LGFUS. The focal point was at 0 mm. (d) The peak positive and negative pressures were observed at 0 mm concerning the focal point along the axial direction. (e) The peak pressures were observed at 0 mm regarding the focal point along the y-direction. (f) The peak pressures along the z-direction were also observed at 0 mm about the focal point. ....59

Figure 2.10 Comparison of pressure distribution from the geometric focus of LGFUS and

ESWT along one-dimensional axial and radial directions. (a) Axial and Z-radial directions of LGFUS. (b) Axial and Z-radial directions of ESWT shock wave.....63

Figure 3.1 Experimental setup for measuring EEG signals upon brain stimulation of LGFUS generated by CNT composite transducers. (a) Information of Laser system and set up. (b) CNT composite transducer used in experiments. (c) LGFUS signal generated by CNT composite transducer. (d) EEG electrode set up. The Red circles is EEG measurement sites, green circle is targeting position of LGFUS. (e) Experimental sequence for real-time monitoring of EEG signals during brain stimulation by LGFUS.(f) EEG monitoring before and after LGFUS stimulation. ....70

Figure 3.2 (a) Measurement set up for LGFUS from laser-generated by CNT composite transducer (Laser energy : 300 and 350 mJ, PRF : 1 and 2 Hz, Wavelength : 532 nm). (b) LGFUS signal and (c) Spectrum when laser energy is 350 mJ. ....72

Figure 3.3 PSD comparison of 3 channels before and after LGFUS stimulation of EEG signals measured at Rat 1. The thick line is the PSD after stimulation, and the thin line is the PSD before stimulation. ....74

Figure 3.4 Real-time EEG signals generated by brain stimulation of LGFUS from CNT composite transducers. (a) EEG signal according to brain stimulation of LGFUS

when laser energy is 300 mJ and PRF is 1 Hz. (b) Laser energy is 350 mJ and PRF is 1 Hz. (c) Laser energy is 350 mJ and PRF is 2 Hz. ....77

Figure 3.5 Comparison of EEG signals according to LGFUS stimulation conditions. (a) EEG signal before stimulation. (b) EEG signal upon real-time stimulation. (c) EEG signal upon stimulation with sham laser on without CNT composite transducer. ....79

Figure 3.6 Total number of peaks at 30 s intervals before and after LGFUS stimulation of each rat. (a) number of peaks before and after stimulation for Rat 1, (b) Rat 2, and (c) Rat 3. The x-axis shows 5 minutes data divided into 10 sections with 30 second intervals, and the y-axis is the average number of peaks for each section. .... 81

Figure 3.7 PSD of the EEG signal responses of 3 rats in 1-30 Hz band before and after LGFUS stimulation ( $p < 0.001$ ). The dotted line on the vertical axis indicates the PSD section in each theta band and the alpha band. The thick line is the PSD after stimulation, and the thin line is the PSD before stimulation. ....83

Figure 3.8 PSD of the EEG signal responses of 3 rats before and after LGFUS stimulation ( $p < 0.001$ ). (a) Theta(4-7 Hz) band. (b) Alpha (8-12 Hz) band. The thick line is the PSD after LGFUS stimulation, and the thin line is the PSD before LGFUS stimulation. ....85

Figure 3.9 Comparison of the increased EEG signal after LGFUS stimulation and the recovered EEG signal 30 minutes after stimulation. (a) EEG signal measurement setup from before LGFUS stimulation to 30 minutes after stimulation. (b) Spectrogram of EEG signal according to brain stimulation of LGFUS for each experimental part. (c) Comparison was made of the EEG signals measured before and immediately after LGFUS stimulation with those measured during real-time stimulation. (d) Comparison was made of the EEG signals before, immediately after, and 30 minutes after LGFUS stimulation. ....87

Figure 3.10 Autopsy rat brain after LGFUS brain stimulation. (a) LGFUS stimulation area in the rat brain (b) Brain slice of the LGFUS stimulation area .....90

Figure 3.11 H&E-stained brain sections after LGFUS exposure for 3 minutes. ....90

Figure 3.12 Real-time EEG signal change with respect to the focal position of the LGFUS. (a) EEG signal with the LGFUS focus shifted to the rat's brain surface at 250 mJ of laser energy and 1 Hz of PRF. (b) EEG signal with the focus of the LGFUS shifted to the rat's cortical bone. ....93

Figure 4.1 (a) Sound speed and density distribution extracted from CT images of the center of the skull cadaver. (b) Measurement setup before and after skull penetration of LGFUS generated from a CNT composite transducer.....100

Figure 4.2 The signal generated by the CNT composite transducer before and after LGFUS penetration into the human skull cadaver. (a) LGFUS measured before cadaver penetration, (b) spectrum. (c) LGFUS measured after human skull cadaver penetration, (d) spectrum. ....102

Figure 4.3 The focal position of LGFUS changes during human skull cadaver penetration.....103

Figure 4.4 The signal generated by the CNT composite transducer before and after the penetration of LGFUS into the human skull cadaver. The signal generated by the CNT composite transducer before and after the penetration of LGFUS into the human skull cadaver, and (b) Developed CNT composite transducer. (c) The pulse wave generated by a HIFU transducer similar to the characteristics of LGFUS.....106

## LIST OF TABLES

Table 1 Averaged acoustic pressure of LGFUS according to different backing at 700 mJ of laser energy. ....	50
Table 2 The frequency spectrum as a function of the diameter of the CNT composite transducer. ....	53
Table 3 Averaged acoustic pressure of LGFUS according to diameter of CNT composite transducer. ....	53
Table 4 $R^2$ , intercept, and slope values for 2, 5, and 8 cm diameter of CNT composite transducers for both positive and negative pressure in Figure 2.7. ....	54
Table 5 Difference in power before and after the LGFUS stimulation of 3 rats measured in 3 channels. Areas with a difference of 15 dB or more before and after stimulation are shaded; Power = (Integrated PSD <sub>AFTER</sub> - Integrated PSD <sub>BEFORE</sub> )/Hz. ....	75
Table 6 Characteristics of LGFUS with and without human skull cadaver penetration. ....	103

# **Laser-Generated Focused Ultrasound for Brain Stimulation Using Carbon Nanotube Composite Transducer**

Jooho Lee

Faculty of Earth and Marine Convergence, Major of Ocean System

The Graduate School

Jeju National University

## **Abstract**

Focused Ultrasound (FUS) can non-invasively and precisely intervene in key circuits that control common and challenging brain disorders. Neurons can be activated or inhibited by adjusting the parameters of FUS. However precise targeting at the microscopic level requires a spatial accuracy of several millimeters. Therefore, the development of high precision neurostimulation is essential to stimulate specific brain regions effectively.

Laser-generated focused ultrasound (LGFUS) has shown potential for precision therapeutic ultrasound applications due to its ability to generate high-pressure, broadband shock waves with a narrow focal spot. However, there has been little research on neurostimulation using shock waves with pulse durations of sub microseconds. Our study thoroughly explores the potential of neurostimulation by LGFUS using carbon nanotube (CNT) composite transducers and presents LGFUS as an excellent precision tool for brain stimulation.

In this study, we explore the structural properties of CNT composite transducers as LGFUS tools to achieve high-precision neuromodulation. To comprehensively investigate the LGFUS properties, CNT composite transducers with different diameters and support structures were fabricated. The peak positive and negative sound pressure generated by the CNT composite transducer are 32 to 52 MPa and -9 to -24 MPa for 2 to 8 cm diameters, respectively. Our experiments confirmed a correlation between increasing transducer diameter and increasing peak pressure in LGFUS.

We investigated responses to rat brain stimulation with LGFUS generated from the explored CNT composite transducers. Electroencephalographic (EEG) signals recorded from rat brains before and after LGFUS stimulation show distinct differences in time and frequency domains. After stimulation, the EEG signal has increased, indicating increased neural activity and distinct changes in the 1-30 Hz band. These changes in the EEG signal highlight the ability to accurately stimulate the brain with LGFUS generated by CNT composite transducers. Finally, as a preliminary experiment to confirm the possibility of human brain stimulation, the possibility of LGFUS penetration into the human cadaver skull was investigated. The peak positive sound pressures before and after skull penetration were 14.6 MPa and 1.1 MPa, respectively, and the central frequency was changed from 1 MHz and 464 kHz, respectively.

These results of LGFUS have important implications for future neurostimulation research and transcranial applications, suggesting potential use for high-precision brain stimulation.

# Chapter I

## INTRODUCTION

### 1.1 Background of Therapeutical Ultrasound

Ultrasound (US) refers to sound waves with frequencies exceeding the audible frequency band ( $>20$  kHz). These high-frequency waves are beyond the range of human hearing. The applications of US have substantially contributed to medical advancements since the mid-20th century.

US is considered one of the safest and most versatile diagnostic modalities in medicine. Focused US (FUS) is focused by a curved transducer, lens, or phased array. It exerts maximum pressure on a small target and much less pressure elsewhere. While the therapeutic potential of FUS has been recognized for decades, its clinical treatments have recently been recognized. FUS has been approved for the treatment of a variety of conditions, including uterine fibroids and lesions of the breast, prostate, and liver. (Aubry et al., 2013, Tempny et al., 2011). The skull, which attenuates and distorts ultrasound transmission, has traditionally impeded applications in the brain. However, over the past few decades, technological, imaging, and medical advances have increased interest in FUS as a significant brain intervention affecting brain structure and function (Figure 1.1). In the 1950s, individuals such as Russell Meyers, Peter Lindstrom, and William and Francis Fry led initial experiments using FUS for the

treatment of movement and mental disorders, as well as brain tumors(Meyers et al., 1959, Nelson et al., 1959). Lars Leksell also penned articles on the application of ultrasound in the central nervous system (CNS) and showed particular interest in using FUS (Leksell, 1956) to treat mental disorders before he developed radiosurgery for non-invasive resection (Jagannathan et al., 2009). These early attempts to deliver FUS to the brain required a craniectomy, with the ultrasound treatment performed in the operating room before the skull bone was replaced. The skin flap over the craniectomy provided a window for repeated FUS hyperthermia treatments and thermal ablation of tumors (Ram et al., 2006). Over the past two decades, several advancements have accelerated research activity in the FUS field. The feasibility of transcranial FUS was realized in early this century by implementing phased array transducers and real-time MRI temperature measurement monitoring (Hynynen et al., 2006). Recently, research has been conducted to treat Alzheimer's disease and Amyotrophic lateral sclerosis by opening the blood-brain barrier using transcranial-FUS. The introduction of therapeutic ultrasound is being studied extensively as an alternative to resection, which is associated with high morbidity and mortality and suppression of the patient's immune system. FUS is a non-invasive method and is of interest in many research areas due to its relatively high safety and low side effects.

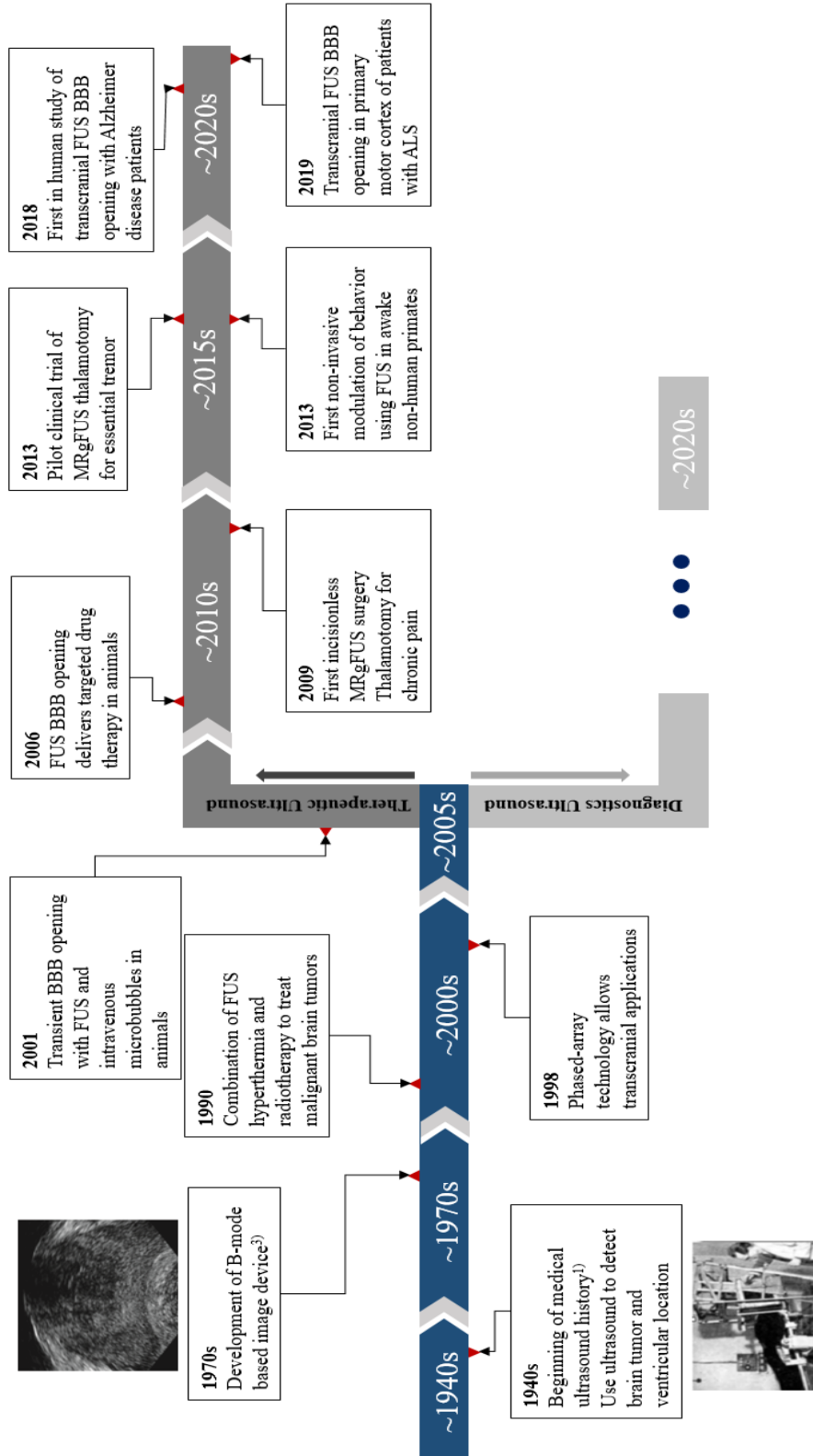


Figure 1.1 Historical development sequence and research trends of therapeutic ultrasound.

Therapeutic ultrasound can be classified into many ways such as intensity or mechanism. One of them is pulse duration combined with intensity and mechanism as illustrated in Figure 1.2. Therapeutic ultrasound can be categorized into continuous waves and pulsed waves, with the latter being most utilized in research. Pulsed waves can be further divided into high-intensity focused ultrasound (HIFU) and low-intensity focused ultrasound (LIFU), both of which serve different research purposes. HIFU is mostly used as thermal ablation, which elevates the temperature of body tissues, leading to cell necrosis in the targeted tissue due to the heat (Pinton et al., 2012, Pernot et al., 2004). It also facilitates drug delivery through the opening of the Blood-Brain Barrier (BBB), a process induced by the cavitation effect (McDannold et al., 2005). LIFU, on the other hand, is employed in neuromodulation and neurostimulation research. It makes use of the acoustic radiation force at a lower intensity than HIFU. In neuromodulation research, studies are being conducted to understand brain functions by observing movements of the tail (King et al., 2013), limb (Lee, W. et al., 2016), and eyeball (Kim, H. et al., 2012) in experimental animals, which are induced by cortex stimulation with LIFU. Neurostimulation research focuses on investigating the responses of cells, tissues, neurons, etc.(Tyler et al., 2008, Tufail et al., 2010), when stimulated by FUS. Based on these findings, LIFU is applied in clinical research for treating conditions like tremors and depression (Bronstein et al., 2011).

In the realm of therapeutic ultrasound, there are types of FUS that have shorter wave characteristics than the traditional pulse waves. These include histotripsy, lithotripsy shock

waves, and laser-generated focused ultrasound (LGFUS). Histotripsy is a non-invasive, non-thermal therapeutic ultrasound technique used to treat various medical conditions (Xu et al., 2021). It relies on the mechanical effect of ultrasound waves at the cellular level to destroy tissue (Xu et al., 2021). This is achieved by using short bursts of ultrasound waves to create controlled cavitation bubbles within the target tissue, which then collapse and cause mechanical destruction of the tissue cells. Shock waves is usually used in lithotripsy. This procedure uses focused shock waves or ultrasound waves to break down stones into tiny pieces, which can then be passed out of the body through the urine (Lingeman et al., 2009). This can be performed non-invasively, as in Extracorporeal Shock Wave Lithotripsy (ESWL).

Transcranial pulse stimulation (TPS) is a brain stimulation method using shock waves (Beisteiner et al., 2020). TPS is specifically developed for clinical applications and is based on single ultrashort ultrasound pulses (3  $\mu$ s) repeated every 200–300 ms. For brain therapy using TPS, this enables a controlled modulation of a specific brain region without unwanted co-stimulations of other brain areas. Comparable to FUS, TPS is applied for several minutes to achieve neuromodulatory effects (Beisteiner et al., 2023). Although size of stimulation foci depends on transducer design and frequency, typical foci are cigar shaped with a length of around 3–5 cm and a width of about 4 mm full width at half maximum (FWHM) (Beisteiner et al., 2020). TPS has characteristics that enable higher precision targeting than the existing FUS. If the area

of brain stimulation is minimized, high safety and high precision are guaranteed with minimal side effects, so research on high-precision FUS is needed.

LGFUS has higher precision characteristics than the TPS and FUS. LGFUS is a single ultrashort pulse and much shorter than TPS. LGFUS is a technique that uses laser-generated thermoelastic expansion to produce FUS waves. This method has several advantages over the traditional ultrasound generation techniques. Firstly, LGFUS can get a broad frequency range with extremely short pulse (~200 ns), which results in improved spatial resolution (Buma et al., 2001, Baac et al., 2012). This makes LGFUS particularly suited for precise targeting of small areas, an application that is of great interest in medical treatments such as targeted drug delivery or non-invasive surgeries (Baac et al., 2012). Secondly, LGFUS offers the advantage of being non-contact, meaning that the generation of ultrasound does not rely on the physical contact between the transducer and the medium (Lee, T. et al., 2018).

FUS technologies used for neurostimulation must be capable of precise targeting without causing tissue damage (Heo et al., 2021, Krishna et al., 2018). LIFU, TPS and LGFUS are among the technologies that meet these requirements. These types of FUS can modulate neuronal activity in specific brain areas. This modulation can potentially provide therapeutic applications for various neurological and psychiatric disorders. For instance, FUS waves on certain parts of the brain can alter the electrical activity of neurons in those areas (Tufail et al., 2010). This could potentially provide relief for conditions such as chronic pain, depression, and neurodegenerative diseases (Baek et al., 2017). With its capacity for targeted stimulation

and minimal side effects, this technique shows promise and could be a useful tool in treating various conditions. This thesis focuses on neurostimulation by LGFUS.

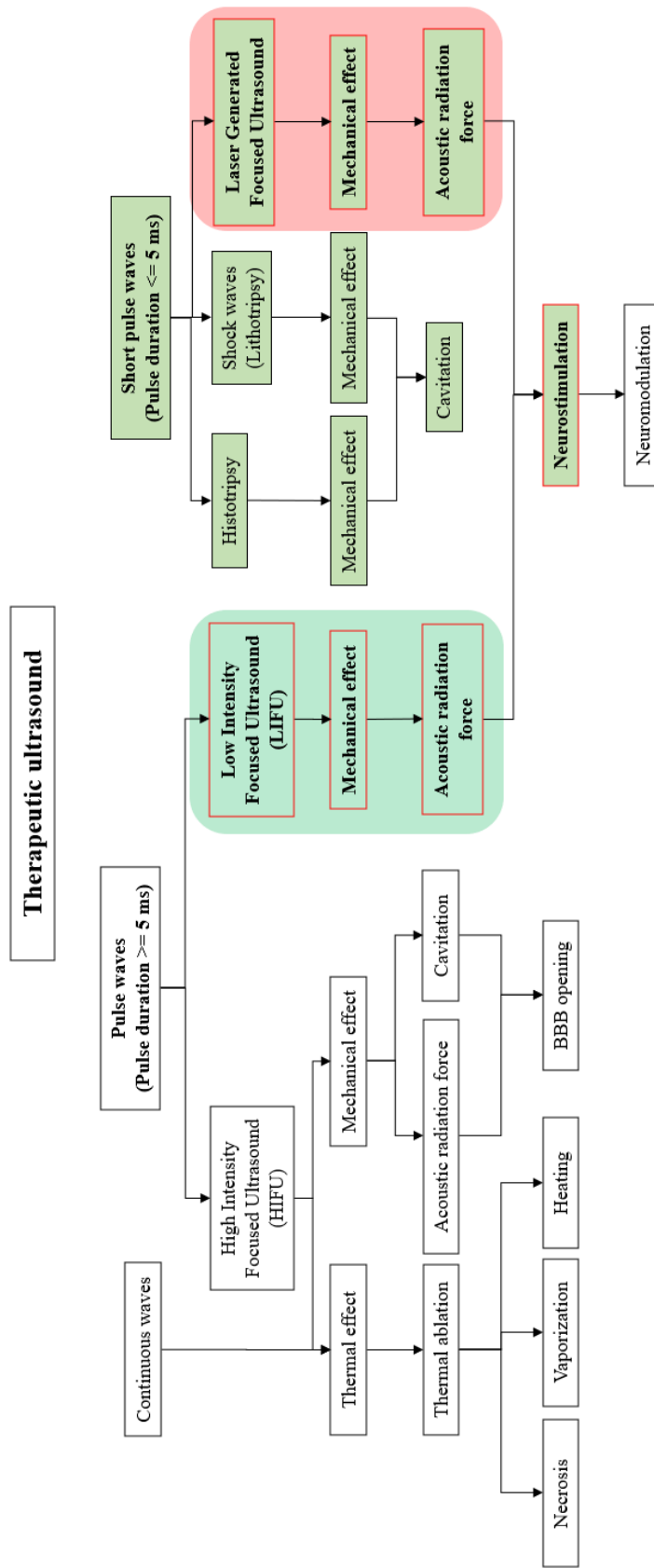


Figure 1.2 Types according to characteristics, mechanism, and application of therapeutic ultrasound.

## 1.2 Neuromodulation of Therapeutic Ultrasound

Neuromodulation has emerged as a treatment approach for neurological disorders. Deep brain stimulation (DBS) (Ashkan et al., 2017) and vagus nerve stimulation (VNS) (Theodore and Fisher, 2007) have been utilized for several decades as invasive treatments for these disorders. However, to mitigate the potential side effects associated with invasive methods, noninvasive brain stimulation techniques such as transcranial magnetic stimulation (TMS) (Kobayashi and Pascual-Leone, 2003, Barker et al., 1985) and transcranial direct-current stimulation (tDCS) (Nitsche and Paulus, 2000, Horvath et al., 2015) have been employed to treat neurological disorders and regulate cortical brain functions (George and Aston-Jones, 2010, Fregni and Pascual-Leone, 2007). Although these electromagnetic stimulation methods offer noninvasiveness, the stimulation area tends to be relatively large compared to the target size, and their ability to reach deep brain regions is limited (Fregni and Pascual-Leone, 2007, Loo and Mitchell, 2005).

In contrast, FUS has the capability to deliver acoustic energy precisely to localized brain regions, including deep brain structures. Low intensity transcranial focused ultrasound (tFUS) has demonstrated the ability to stimulate brain functions without causing temperature elevation or thermal ablation, thus minimizing potential side effects (Fry et al., 1958, Kim, H. et al., 2014, Yoo et al., 2011). Compared to noninvasive techniques, low intensity tFUS provides enhanced spatial resolution and can effectively target deeper areas. The energy of acoustic pulse waves is transmitted through the skull, and the target's position can be adjusted using

phase correction with multi-element array systems. Moreover, the parameters of FUS can be adjusted to induce nerve activation or inhibition (Kim, H. et al., 2014, King et al., 2013).

FUS has different characteristics depending on its parameters. Neuromodulation using continuous or short, long-pulse ultrasound waves has also been explored (Tsui et al., 2005, Foley et al., 2007). Various parameters, such as ultrasound fundamental frequency ( $f_0$ ) (Ye et al., 2016), ultrasound duration (UD)(King et al., 2013), duty cycle (DC) (Plaksin et al., 2016, Kubanek et al., 2018), and pulse repetition frequency (PRF) (Kubanek et al., 2018), have been studied in ultrasound neuromodulation. To optimize the intensity, UD, and PRF for successful neuromodulation, it is necessary to evaluate the characteristics of ultrasound. Studies have observed motor responses elicited at minimum threshold acoustic intensities with specific ultrasound parameters ( $f_0 = 350$  kHz, UD = 300 ms, etc.) (Kim, H. et al., 2014) . The success rate of neurostimulation has also been examined about ultrasound characteristics such as frequency band, acoustic intensity, and UD (King et al., 2013). Many studies have investigated the key parameters of ultrasound stimulation by controlling intensity, PRF, and pulse duration (King et al., 2013, Kim, H. et al., 2014). Research using pulsed ultrasound for neurostimulation has shown a low success rate when the acoustic intensity and duration parameters fall below specific threshold values. For instance, when the intensity is less than  $4.2 \text{ W/cm}^2$ , the success rate of ultrasound stimulation is below 66%. Similarly, when the sonication duration is less than 80 ms, the success rate is below 77% (Kim, H. et al., 2014, King et al., 2013).

While LIFU holds promise in the realm of neurostimulation and neuromodulation, it has

limitations, specifically in reducing pulse width and minimizing side effects during the adjustment of acoustic parameters. LGFUS, on the other hand, employs laser-induced thermoelastic expansion to generate high-frequency focused ultrasound waves. Much like LIFU, LGFUS can stimulate tissue by exerting a mechanical effect. LGFUS distinguishes itself from LIFU in its operation with significantly shorter pulse length and its induction of a non-thermal effect. This means that LGFUS can deliver precise stimulation while operating without posing the risk of thermal damage to tissues, a potential concern associated with other types of ultrasound. While LGFUS is still in the early stages of research and development, its potential for non-invasive, precise, and safe neuromodulation makes it a promising technology for future neurostimulation applications.

### 1.3 Characteristics of LGFUS

Shock waves have also been applied in brain-related treatments. With their wide frequency band and short rising time of a few microseconds, shock waves have been used to verify BBB opening in lithotripsy (Kung et al., 2018). Additionally, the stability and efficacy of creating targeted lesions in the brain have been demonstrated using histotripsy (Xu et al., 2021).

LGFUS transducers have shown promise in precise therapeutic ultrasound applications, as they can produce high-pressure, high-frequency shock waves with a tight focal spot, resulting in localized acoustic exposure (Baac et al., 2012). LGFUS transducers have been employed in various high-precision therapies, including lithotripsy (Kim, J. et al., 2016), cell manipulation (Baac et al., 2013), remotely controlled drug delivery (Di et al., 2015). However, there have been limited studies on neurostimulation using shock waves generated by LGFUS.

LGFUS has emerged as a promising alternative to other modalities for generating ultrasound signals, such as electric, electromagnetic, and piezoelectric methods (Buma et al., 2001). LGFUS has shown great potential in providing a superior non-invasive approach for therapeutic purposes and various biomedical applications (Lee, T. et al., 2018). The key mechanism behind LGFUS is the thermoelastic effect, also known as the photoacoustic or optoacoustic effect (Li, J. et al., 2019). This involves the conversion of laser energy into acoustic energy using the thermal and elastic properties of the materials used in ultrasound transducer fabrication. Another notable attribute of LGFUS is its ability to generate shock

waves at the focal point, akin to the process in shock wave lithotripsy (Baac et al., 2012), using specially designed photoacoustic composite transducers to efficiently convert laser energy into acoustic energy (Lee, T. et al., 2018).

Optoacoustic transducer has been investigated using different materials and techniques to generate shock waves and to understand the effect of various physical parameters on LGFUS characteristics. CNT composite transducers are a promising modality in the field of optoacoustic transducers due to their exceptional heat conduction and expansion properties. Baac et al. utilized optoacoustic lenses of small diameters (6 mm and 12 mm) to determine the focal waveform's peak positive and negative pressure, achieving a maximum positive pressure of over 50 MPa (Baac et al., 2012). However, no study has yet examined the characterization of shock waves using composite transducers with more practical sizes (up to 8 cm of diameter) for transcranial applications through human skull. LGFUS has not yet been explored for neurostimulation utilizing these properties including the effects of structure of the CNT composite transducers on shock wave characteristics.

CNT composite transducers can be used in different applications due to their exceptional heat conduction and expansion properties. They can generate high optoacoustic pressure at the focal point. Therefore, optoacoustic transducers are another effective way of generating shock waves with similar or improved properties in different applications with improved performance.

## 1.4 Motivation

Brain stimulation using FUS has been a field attracting extensive research in a recent decade. It's being utilized as an effective treatment tool for various brain diseases, to the extent that is being used in clinical research for treatment. Nonetheless, FUS has its limitations. As the brain is the most sensitive and vital organ in the body, precisely targeting ultrasonic waves for stimulation is a key. After ultrasound waves penetrate the human skull, distortion of the focus position and attenuation of the ultrasound output occurs. A transducer array is used to correct the distorted focus using techniques such as beamforming or acoustic ray tracing, based on the skull's characteristics to accurately target the focal position after penetrating the skull.

However, for microstimulation of a specific brain region, the beam size at the focal point must be reduced. Parameters such as the ultrasound frequency band, pulse duration, and energy intensity are adjusted to decrease the beam size. While adjusting these ultrasound parameters enables precise microstimulation of brain regions at specific locations, it is challenging to form a focus of less than a few millimeters by adjusting the parameters alone.

The potential of LGFUS in brain stimulation is a fascinating field of research, marked by several key differences and advantages over traditional FUS techniques.

First and foremost, LGFUS possesses superior spatial resolution owing to its wide frequency band and extremely short pulse waves. This makes it particularly adapt at targeting smaller areas with greater precision, a feature not easily achieved with conventional FUS. Such precise targeting is paramount when stimulating specific brain areas, a delicate and complex

organ. This technological advantage could potentially lead to breakthroughs in exploration of the brain function map and the treatment of various brain disorders, making LGFUS a promising tool in neurotherapeutic applications.

Second, using LGFUS opens new avenues for research into brain stimulation responses to ultrasound stimulation. While there are currently limited applications in this area, the unique properties of LGFUS make it a promising candidate for future investigations. Understanding the response to LGFUS stimulation in the brain tissue could provide invaluable insights into the effects of ultrasound on the brain, potentially leading to more effective and safer therapeutic interventions.

In summary, the unique properties and potential of LGFUS make it a compelling area of research in the field of brain stimulation, offering several advantages and opportunities over traditional FUS techniques.

## 1.5 Specific Aims

This study aims to assess the feasibility of brain stimulation using LGFUS and is organized into three specific objectives.

The first objective is to fabricate and evaluate a CNT composite transducer capable of producing LGFUS. This aspect of the study focuses on understanding the characteristics of LGFUS, particularly in terms of the structure of the backing body onto which the composite is coated and the diameter of the transducer. These factors have not been evaluated in previous LGFUS studies and could offer significant insights into the generation and control of LGFUS.

The second objective is to observe the changes in brain signals when the brains of small animals are exposed to LGFUS. To assess whether brain is stimulated by LGFUS through the skull of a small animal, an EEG device is non-invasively attached to the rat's head. An experimental setup has been established that allows for the reception of brain EEG signals during and pre- and post-LGFUS stimulation. This objective aims to provide an observation of the impact of LGFUS on brain activity.

The third one is to verify the output of LGFUS after it penetrates the human skull. This is a preliminary experiment aimed at confirming the capacity of LGFUS to stimulate the human brain. To investigate the characteristics of LGFUS pre- and post-penetration through the human skull, an experimental setup was established to measure acoustic signals using a needle-type hydrophone. This objective seeks to establish the practicality and potential of LGFUS in human applications.

In summary, these specific aims provide a comprehensive approach to understanding the potential of LGFUS in brain stimulation, from the generation of LGFUS using a novel transducer to its application in small animals and preliminary investigations in humans.

## 1.6 Thesis Outline

This thesis is structured into five chapters, including introduction, three experimental studies, and conclusion.

Chapter 1 introduces the research, presenting the background, necessity, motivation, and aims of this study.

Chapter 2 delves into the principle of LGFUS and illustrates the performance variability according to different structures of the CNT composite transducer. It provides validation based on the backing structure and diameter of the CNT composite transducer. The results suggest the potential for optimized LGFUS in applied research, which can be achieved by identifying an optimal CNT composite transducer to generate LGFUS.

Chapter 3 investigates the feasibility of using LGFUS, generated from a CNT composite transducer, for brain stimulation. It confirms the brain signals activated when LGFUS stimulates the brain area corresponding to a rat's somatosensory, using EEG equipment. To further investigate the effect of LGFUS stimulation, EEG signals recorded before, during, and after stimulation are analyzed.

Chapter 4 provides a preliminary experiment to explore the characteristics of LGFUS after it has penetrated the human skull. It confirms the possibility of brain stimulation post-penetration into a human skull cadaver.

Finally, Chapter 5 concludes the study, summarizing the key findings, and proposing future avenues for research.

## **Chapter II**

# **LASER GENERATED FOCUSED ULTRASOUND AND TRANSDUCER STRUCTURE**

### **2.1 Background**

The composite transducers consist of a high optically absorptive material and an elastomeric polymer grown on a substrate (Buma et al., 2001). The high optical absorbing material is essential for maximum light absorption with minimal reflection, while the elastomeric polymer with high thermal expansion coefficient converts this absorbed energy into high amplitude acoustic energy (Buma et al., 2001, Miranda et al., 2021). Carbon nanotubes (CNTs) are a high absorptive material and generate localized high temperatures under laser irradiation (Chang et al., 2015). In addition, CNTs enhance peak pressure by reducing reflection and increasing maximum optical absorption, exceeding the performance of metals by more than an order of magnitude (Shi et al., 2011, Hsieh et al., 2015). When pulsed laser excitation is applied, CNT composites generate extreme acoustic pressure, surpassing films of chromium (Cr) or gold nanoparticles with the same elastomeric polymer (Won Baac et al., 2010). In addition, due to the nanometer-scale structure of CNTs, rapid heat diffusion to the surrounding medium occurs (Baac et al., 2012). This unique property allows

thermal energy to be transferred to the adjacent expanding layer. Polydimethylsiloxane (PDMS) is commonly used as the thermally expanding layer due to its high thermal coefficient of volume expansion ( $\alpha = 0.92 \times 10^{-3} \text{ K}^{-1}$ ) (Chang et al., 2015). Consequently, when CNTs are heated, they quickly transfer most of the absorbed thermal energy to the adjacent PDMS layer, resulting in rapid thermal expansion with high amplitude (Baac et al., 2012). Baac et al. confirmed that CNT-PDMS films can withstand higher optical fluence than chromium (Cr) films, making them ideal composite films for maximum optoacoustic excitation (Won Baac et al., 2010). LGFUS with a CNT and PDMS composite transducer on a concave surface can generate high frequency ( $>15 \text{ MHz}$ ) ultrasound with an acoustic pressure exceeding 50 MPa from a single element lens (6 mm diameter) (Baac et al., 2012). The laminated structure of these films defines them as excellent materials for generating high amplitude, high frequency ultrasound (Baac et al., 2015).

Colchester et al. employed functionalized CNTs dissolved into a PDMS solvent and coated them onto a substrate, using planar optical fibers as the substrate and achieving maximum pressures of 3.6 MPa and 4.5 MPa (Colchester et al., 2014). Additionally, experiments with CNTs of different diameters and lengths were conducted to study the effect of CNT thermal conductivity on the performance of optoacoustic transducers, resulting in CNTs with a diameter of 8 nm and a length of 10–30  $\mu\text{m}$  (Li, J. et al., 2019). Yixuan et al. investigated CNT-PDMS composites with different thicknesses on pure PDMS to identify better-performing transducers, observing a decrease in thermal conductivity with a reduction

in CNT film thickness (Li, Y. et al., 2019). In another study, the characteristics of LGFUS were evaluated using a perforated photoacoustic lens, achieving a peak positive pressure of 46.5 MPa (Heo et al., 2021). These studies have provided valuable insights into the CNT-PDMS composite structure and its impact on LGFUS characteristics. However, no study has yet examined the characterization of LGFUS using composite transducers with larger diameters (up to 8 cm) which is practical for human brain applications to understand their relative effects on LGFUS properties. LGFUS has not yet been explored for neurostimulation utilizing these properties.

This study examines the impact of altering the diameter and backing structure of a CNT-PDMS composite transducer on the peak amplitudes and characteristics of LGFUS. The CNT composite transducer with highest peak pressures is investigated by measuring LGFUS according to the backing structure. The areas of interest include the maximum positive and negative pressure generation of LGFUS at the focal point using larger diameters compared to previous studies. The purpose of changing diameters is to fabricate transducers with more suitable sizes and peak pressures at the focal point. Although smaller diameters are advantageous for cell culture studies, miniature composite transducers cannot be effectively utilized for further investigation of LGFUS effects, as well as acoustic attenuation and impedance, in transcranial brain applications. Therefore, this study aims to construct a CNT composite transducer with maximum pressure generation using more practical diameters.

## 2.2 Principles of LGFUS

The sound waves generated by laser energy is due to the thermoelastic effect of the medium. The thermoelastic effect is a phenomenon that causes deformation when an arbitrary heat source changes the temperature of a solid medium with elastic properties. The following heat conduction equation determines the temperature distribution within the medium due to this phenomenon (Wetsel, 1986).

$$\rho C_f \frac{\partial T}{\partial t} + \nabla \cdot q = Q \quad (2.1)$$

In the formula,  $\rho$  is density,  $C_f$  is specific heat,  $T$  is temperature, and  $q$  is heat flux which is given by the thermal conductivity  $k$  as

$$q = -k\nabla T \quad (2.2)$$

The size of the heat source  $q$  is the energy generated per unit time in unit volume and depends on the laser pulse waveform. Meanwhile, the deformation of an object that occurs due to temperature changes is accompanied by elastic deformation and inelastic deformation. Thermal strain  $\varepsilon^{th}$ , which is an inelastic strain, is given by the thermal expansion coefficient  $\alpha$  as follows.

$$\varepsilon^{th} = \alpha\Delta T \quad (2.3)$$

In a rectangular coordinate system  $\vec{u}(u, v, w)$

$$\varepsilon^{el} = \begin{pmatrix} \frac{\partial u}{\partial X}(-\alpha\Delta T) & \frac{1}{2}\left(\frac{\partial v}{\partial X} + \frac{\partial u}{\partial Y}\right) & \frac{1}{2}\left(\frac{\partial w}{\partial X} + \frac{\partial u}{\partial Z}\right) \\ \frac{1}{2}\left(\frac{\partial v}{\partial X} + \frac{\partial u}{\partial Y}\right) & \frac{\partial v}{\partial Y}(-\alpha\Delta T) & \frac{1}{2}\left(\frac{\partial w}{\partial Y} + \frac{\partial v}{\partial Z}\right) \\ \frac{1}{2}\left(\frac{\partial w}{\partial X} + \frac{\partial u}{\partial Z}\right) & \frac{1}{2}\left(\frac{\partial w}{\partial Y} + \frac{\partial v}{\partial Z}\right) & \frac{\partial w}{\partial Z}(-\alpha\Delta T) \end{pmatrix} \quad (2.4)$$

And the stress  $S$  according to elastic strain is obtained as follows.

$$S = C : \varepsilon^{el} \quad (2.5)$$

Here,  $C$  the elastic stiffness coefficient is a fourth-order tensor with components of  $6 \times 6$ , and ‘:’ represents the double scalar product between the fourth-order tensor and the second tensor.

For isotropic solids, the elastic stiffness coefficient  $C$  is given by Young's modulus  $E$  and Poisson's ratio  $\sigma$  (Auld, 1973). Then,

$$S = \frac{E}{(1+\sigma)(1-2\sigma)} \times \left( \begin{array}{ccc} (1-\sigma) \frac{\partial u}{\partial X} + \sigma \left( \frac{\partial v}{\partial Y} + \frac{\partial w}{\partial Z} \right) - (1+\sigma)\alpha\Delta T & \frac{(1-2\sigma)}{4} \left( \frac{\partial v}{\partial X} + \frac{\partial u}{\partial Y} \right) & \frac{(1-2\sigma)}{4} \left( \frac{\partial w}{\partial X} + \frac{\partial u}{\partial Z} \right) \\ \frac{(1-2\sigma)}{4} \left( \frac{\partial u}{\partial Y} + \frac{\partial v}{\partial X} \right) & (1-\sigma) \frac{\partial v}{\partial Y} + \sigma \left( \frac{\partial u}{\partial X} + \frac{\partial w}{\partial Z} \right) - (1+\sigma)\alpha\Delta T & \frac{(1-2\sigma)}{4} \left( \frac{\partial w}{\partial Y} + \frac{\partial v}{\partial Z} \right) \\ \frac{(1-2\sigma)}{4} \left( \frac{\partial u}{\partial Z} + \frac{\partial w}{\partial X} \right) & \frac{(1-2\sigma)}{4} \left( \frac{\partial v}{\partial Y} + \frac{\partial w}{\partial Z} \right) & (1-\sigma) \frac{\partial w}{\partial Z} + \sigma \left( \frac{\partial u}{\partial X} + \frac{\partial v}{\partial Y} \right) - (1+\sigma)\alpha\Delta T \end{array} \right) \quad (2.6)$$

The equation of motion of an elastic solid for this stress is as follows.

$$\rho \frac{\partial^2 \vec{u}}{\partial t^2} = \nabla \cdot S \quad (2.7)$$

After obtaining  $\nabla \cdot S$  from Eq. (2.6), considering the motion in one axis direction (here, the  $y$  axis), the equation of motion becomes as follows.

$$\rho \frac{\partial^2 \vec{u}}{\partial t^2} = \frac{E}{(1+\sigma)} \times \left( \frac{(1-\sigma)}{(1-2\sigma)} \frac{\partial^2 v}{\partial Y^2} + \frac{1}{4} \left( \frac{\partial^2 v}{\partial X^2} + \frac{\partial^2 v}{\partial Z^2} + \frac{\partial^2 u}{\partial X \partial Y} + \frac{\partial^2 w}{\partial Y \partial Z} \right) + \frac{(1-\sigma)}{(1-2\sigma)} \left( \frac{\partial^2 u}{\partial X \partial Y} + \frac{\partial^2 w}{\partial Y \partial Z} \right) - \frac{(1+\sigma)}{(1-2\sigma)} \frac{\partial}{\partial Y} (\alpha\Delta T) \right) \quad (2.8)$$

In this equation, for isotropic elastic bodies with a Poisson's ratio close to 0.5, the second term on the right side is smaller than the other terms to be ignored. If we consider only the longitudinal wave and ignore the third term, which includes the transverse change, Eq. (2.8) is organized as follows.

$$\rho \frac{\partial^2 v}{\partial t^2} = \frac{E(1-\sigma)}{(1+\sigma)(1-2\sigma)} \frac{\partial^2 v}{\partial Y^2} - \frac{E}{(1-2\sigma)} \frac{\partial}{\partial Y} (\alpha\Delta T) \quad (2.9)$$

In an isotropic elastic solid, the longitudinal wave sound speed  $C_s$  is as follows:

$$C_s = \sqrt{\frac{E(1-\sigma)}{\rho(1+\sigma)(1-2\sigma)}} \quad (2.10)$$

$$\frac{1}{C_s^2} \frac{\partial^2 v}{\partial t^2} - \frac{\partial^2 v}{\partial Y^2} = -\alpha \frac{1+\sigma}{1-\sigma} \frac{\partial T}{\partial Y} \quad (2.11)$$

In the wave equation of Eq. (2.11), the  $-\alpha \frac{1+\sigma}{1-\sigma} \frac{\partial T}{\partial Y}$  on the right side corresponds to the sound source, indicating that the spatial change rate of temperature determined in Eq. (2.1) generates sound waves. It is consistent with the theory (Drain, 2019)). Eq. (2.1) indicates that the temperature change over time at a specific boundary where heat is generated is correlated with the time integral of the laser waveform that causes heat as well as the characteristics of the medium such as specific heat, density, and thermal conductivity, and temperature in Eq. (2.11). It shows that the slope of the temperature distribution formed in the medium when a heat wave that causes a change propagates from the boundary determines the characteristics of the generated sound wave.

The conditions for LGFUS generation are as follows:

- 1) For absorbers, materials like metals or carbon-based substances should have low specific heat capacity to ensure high light-to-heat conversion efficiency.
- 2) Regarding the surrounding medium, materials such as PDMS with significant coefficients of thermal expansion are preferred for optimal heat-to-ultrasound conversion efficiency.
- 3) The size of absorptive materials significantly influences their heat transition to the surrounding medium. Absorbers at nanoscale dimensions permit short thermal diffusion times, which is crucial for high-frequency ultrasound generation. Beyond size considerations, the high thermal conductivity of the absorber and high thermal diffusivity of the surrounding medium aid in optimizing rapid heat transition.

Figure 2.1 illustrates the principle of LGFUS: The laser system generates thermal energy that irradiates onto CNTs. The CNTs absorb this heat energy and transfer it to PDMS, causing it to expand and contract due to this transferred energy; this expansion and contraction generate sound waves. While materials suitable for generating LGFUS have been identified in previous research, LGFUS characteristics can vary based on manufacturing methods and laser system properties. Furthermore, no evaluations have been conducted on structural characteristics beyond those related to the manufacturing material of the LGFUS transducer.

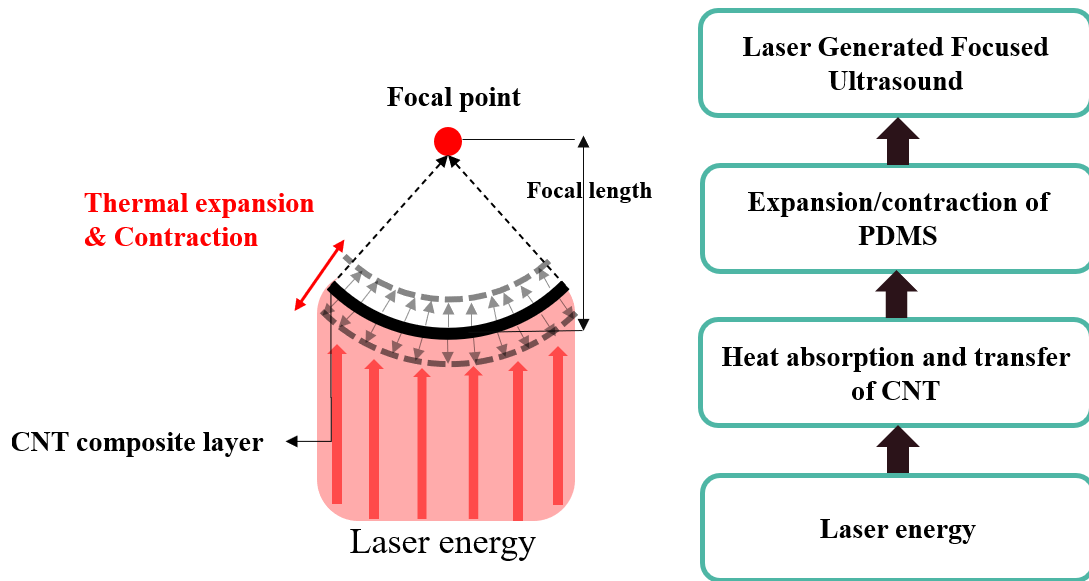


Figure 2.1 The principle of LGFUS transducer and sequence of converting laser energy to shock wave for LGFUS. The CNT composite layer receives the thermal energy of the laser and generates a LGFUS through contraction and expansion.

## 2.3 Materials and Method

### 2.3.1 Fabrication of CNT composite transducer

The manufacturing process of the CNT composite transducer that generates LGFUS is shown in Figure 2.2(a). To fabricate all CNT composite transducers, concave-shaped polymethyl methacrylate (PMMA) was used as a substrate. Multiwalled CNTs (MWCNTs) (purity: 85%wt, 90%wt. refining, diameter: 5~10 nm, length: 10~20 um) (Applied Carbon Nano, Pohang-si, Korea) were used for the thermal conductivity layers. PDMS (SYLGARD 184, Dow Silicones Corporations, Auburn, MI, USA) was used for an elastomeric heat expansion layer. The CNT solution was degassed with a vacuum pump and sprayed evenly onto the surface with a spray coater. The PDMS solution was also degassed, dried at 100 ° C for 1 hour, applied to the CNT solution, and poured evenly into a spin coater at 2000 rotation per minute (RPM) for 2 minutes. Finally, after drying at 100 ° C for one day, if not properly dried, additional drying was required.

Figure 2.2(b) is scanning electron microscope (SEM) image of LGFUS transducer. During the coating and drying process, a composite layer is formed from the CNT and PDMS layers.

### CNT-PDMS composite fabrication process

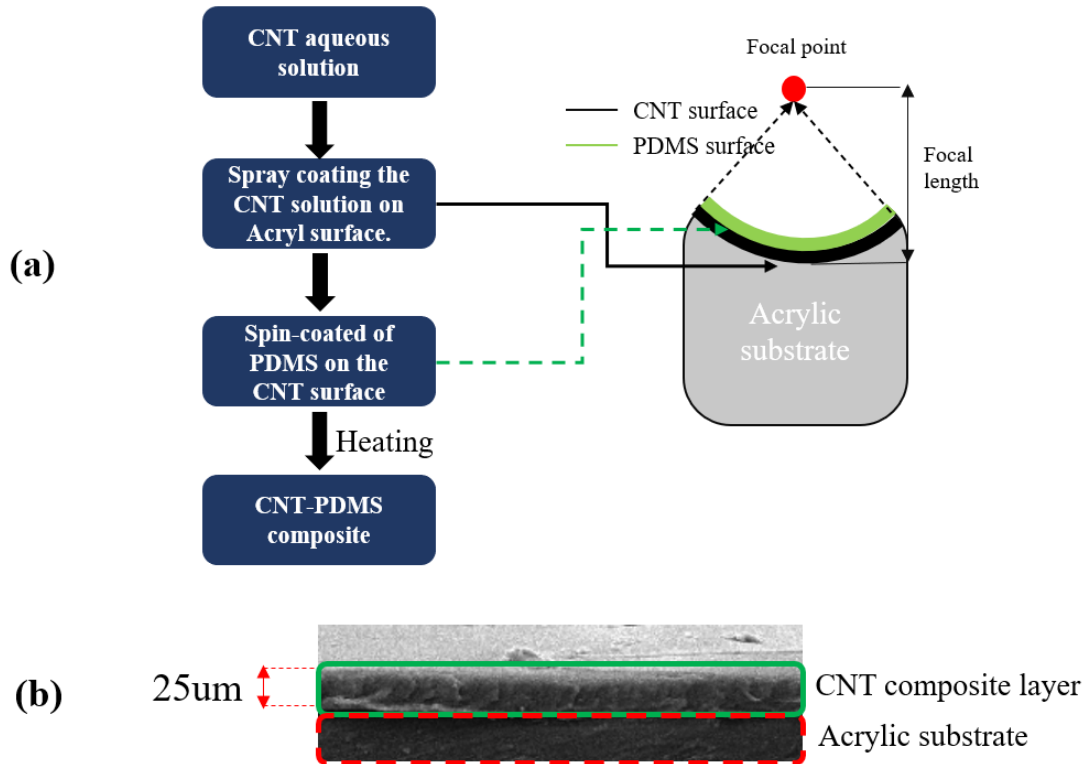


Figure 2.2 (a) The fabrication process of LGFUS transducers. The CNT aqueous solution is spray-coated onto a concave acrylic substrate and dried at room temperature. PDMS is spin-coated onto the surface of the dried CNT layer at 2000 RPM for 2 minutes and dried at 100 °C for 1 hour. (b) SEM image of LGFUS transducer structure. The green box is CNT-PDMS composite layer, and blue box is an acrylic substrate layer.

### 2.3.2 Difference structure of LGFUS transducer

To investigate the characteristics of LGFUS based on the structure of the transducer, we analyzed LGFUS properties to both the backing strength and diameter of the transducer, as illustrated in Figure 2.3. Acoustic pressure generated by expansion and contraction of the PDMS layer radiated toward the focal direction; however, they were not adequately dispersed by acrylic in the opposite direction. To transition from an acrylic backing to alternative materials such as water or air, a 14 mm hole was drilled at the center of a 20 mm diameter acrylic base. Figure 2.3(a) shows the design to allow the PDMS to expand by using backing with water and air. After coating CNT and PDMS onto an acrylic concave lens surface covered with wrap, we removed this CNT composite layer along with its wrap. A CNT composite transducer was then manufactured by attaching this desorbed CNT composite layer onto the edge of a perforated concave lens. The backing layer types include air, water, and rigid acrylic. An exploration of LGFUS characteristics relative to diameter was conducted by applying a CNT composite layer onto an acrylic base with diameters spanning 20 mm, 50 mm, and 80 mm, as shown in Figure 2.3(b).

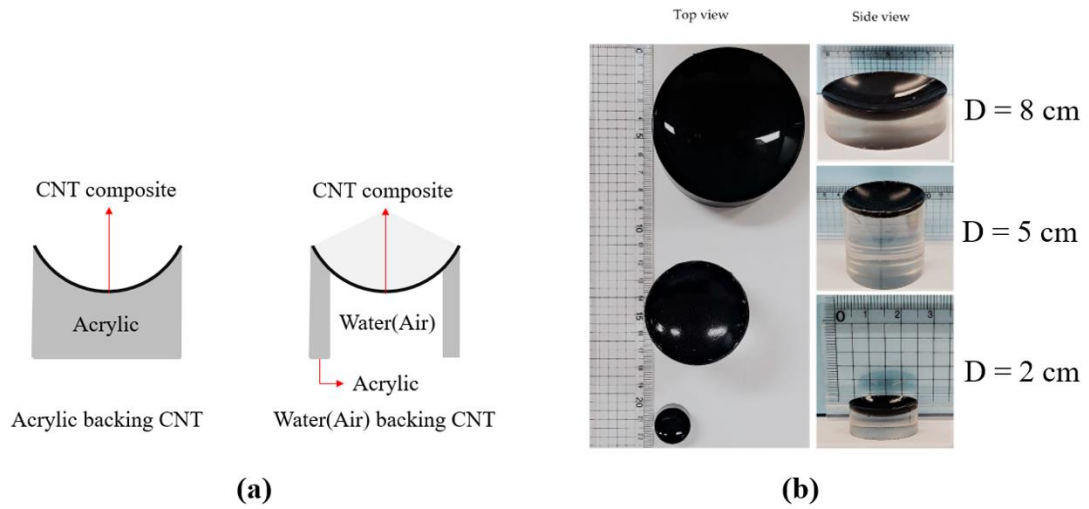


Figure 2.3 The shape of the LGFUS transducer about the backing structure of the transducer substrate and changes in substrate diameter. (a) 20 mm diameter transducer substrate base design that converts acrylic-backing to air and water-backing using a 14 mm hole at the center of the substrate. (b) CNT-PDMS composite transducers of different sizes were used in the experiment. The top view of 8 cm, 5 cm, and 2 cm transducers, along with their side view, are presented.

### 2.3.3 LGFUS Acquisition

The experimental setup for optoacoustic wave signal generation and characterization is illustrated in Figure 2.4. A Q-switched Nd: YAG laser (STL-5000Q, Stratek, Anyang-si, Korea) was employed as an optical source with a wavelength of 532 nm and a pulse repetition frequency of 2 Hz. The diameter of the laser beam was initially 6 mm. It expanded up to 80 mm, increasing the distance from the composite transducer after passing through the beam expander. The composite transducer of interest was mounted inside a degassed water tank and aligned with the laser system. The laser beam has a spatial beam profile of Gaussian distribution with a much higher acoustic pressure at the center than the off-axis location [8]. A 0.2 mm needle hydrophone (NH0200, Precision Acoustics Ltd., Dorchester, UK) was aligned with an acoustic wave generation setup and immersed inside the degassed water tank for the acoustic signal measurement. The needle hydrophone was fixed on an XYZ base with adjustable handwheels to find the focal point and range of the acoustic pressure. The distance of the needle hydrophone from the composite transducer was kept to the focal length of the respective composite transducer. The acoustic wave signal recorded through the needle hydrophone was amplified using a preamplifier (HP Precision Acoustics. Ltd., Dorchester, UK) and fed to an oscilloscope (LT354, Lecroy, New York, NY, USA), which was connected to a personal computer to record the signal data. An external trigger from the laser system was employed to synchronize the time series of laser excitation with the data collected from the oscilloscope. Ultrasound wave signals received by the needle hydrophone were post processed

to calculate the acoustic pressure and investigate for further characterization.

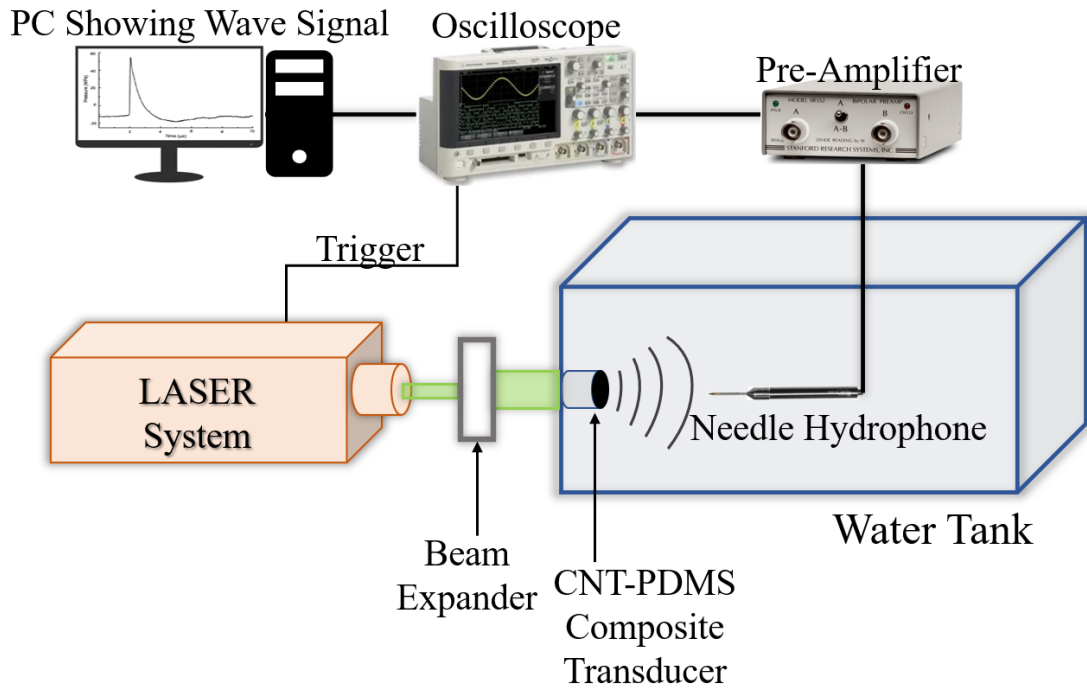


Figure 2.4 Experimental setup for LGFUS generation and measurement. The CNT-PDMS composite transducer was mounted inside a degassed water tank and aligned with the laser system (Q-switched Nd: YAG laser (STL-5000Q, Stratek, Anyang-si, Korea). The needle hydrophone (NH0200, Precision Acoustics Ltd., Dorchester, UK) collected the LGFUS signal generated from the CNTPDMS composite transducer, which was then amplified by a pre-amplifier (HP Precision Acoustics. Ltd., Dorchester, UK) and sent to the oscilloscope (LT354, Lecroy, New York, NY, USA). The signal data from the oscilloscope were fed to a PC for analysis.

## 2.4 Results

### 2.4.1 Structure Changing of CNT Composite Transducer

Figure 2.5 presents an investigation into LGFUS concerning the backing strength of the acrylic base, where the CNT composite layer is affixed. Figure 2.5(a) illustrates the LGFUS signal generated from the CNT composite transducer supported by acrylic, water, and air when the laser energy reaches 700 mJ. Measurements of LGFUS generated in each backing structure according to laser energy revealed peak positive pressures of 26, 8, and 6 MPa for each transducer, respectively, and peak negative pressures of -9, -6, and -5 MPa, respectively. The LGFUS was measured three times for each different type of transducer, and the average pressure was calculated, as shown in the Table 1. As shown in Figure 2.5(b), the positive and negative acoustic pressures increased with the rise in laser energy for all three transducer backing structures. It was observed that the positive and negative sound pressures for CNT composite transducers backed by air and water were significantly lower compared to those with acrylic backing. As the laser energy was increased from 500 mJ to 700 mJ, the negative pressure of LGFUS generated by the acrylic backing transducer satuated to -9.8 MPa.

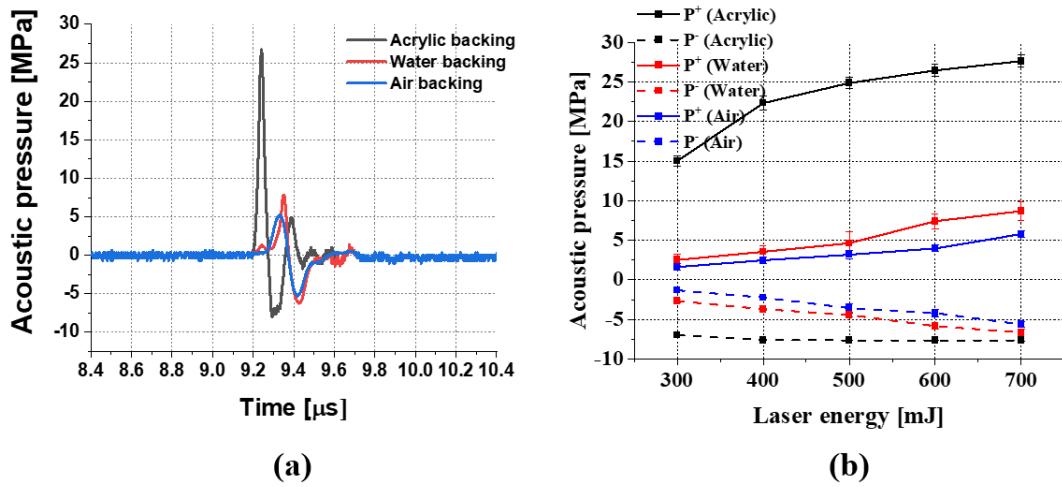


Figure 2.5 Acoustic pressure from CNT composite transducer with laser energy for different backing layer. (a) LGFUS signal generated from the CNT composite transducer supported by acrylic, water, and air when the laser energy of 700 mJ. (b) The positive and negative pressures according to laser energy about all three transducer backing structures.

Table 1 Averaged acoustic pressure of LGFUS according to different backing at 700 mJ of laser energy.

N = 3 At Laser energy = 700 mJ	Acrylic	Water	Air
<b>Peak P+</b>	30.3 $\pm$ 2.84	8.69 $\pm$ 1.17	5.79 $\pm$ 0.46
<b>Peak P-</b>	-8.65 $\pm$ 1.03	-6.64 $\pm$ 0.39	-5.62 $\pm$ 0.30

#### 2.4.2 Acoustic Pressure According to Diameter Changing

An LGFUS was observed at the focal point due to the nonlinear propagation of the wave pulse. Figure 2.6(a)–(c) shows the focal waveforms of the 2 cm, 5 cm, and 8 cm composite transducers, respectively. The positive peak pressures of the LGFUS correspond to 35 MPa, 42 MPa, and 53 MPa, respectively. Their corresponding negative pressures are -10 MPa, -22 MPa, and -25 MPa, respectively. The frequency spectra of these LGFUS signals are shown in Figure 2.6(d)–(f). The center frequencies, peak amplitudes, and -6 dB bandwidth values of the CNT composite transducers are shown in Table 2. The center frequencies are between 4 and 6.5 MHz and the bandwidths are between 6 and 7.8 MHz. Table 3 shows the average sound pressure of the transducer according to diameter.

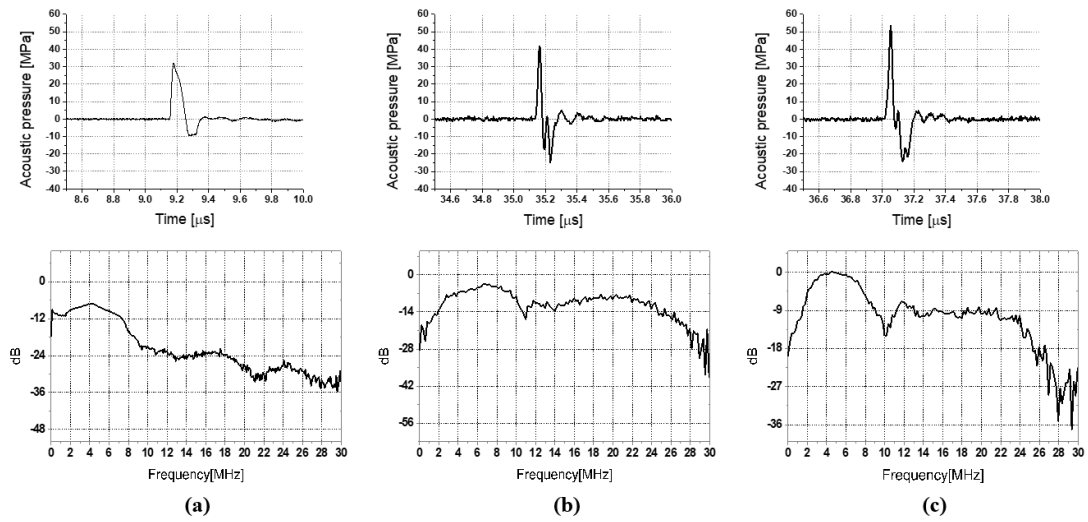


Figure 2.6 Waveforms and their spectra of measured pressure showing the peak positive and negative pressures of the LGFUS generated by CNT composite transducers of different diameters. Figures (a–c) show the time domain signals, while (d–f) shows the frequency domain analysis of the 2 cm, 5 cm, and 8 cm CNT composite transducers, respectively.

Table 2 The frequency spectrum as a function of the diameter of the CNT composite transducer.

	<b>D = 8cm</b>	<b>D = 5cm</b>	<b>D = 2cm</b>
<b>Center frequency</b> [MHz]	4.39	6.78	4.09
<b>-6 dB bandwidth</b> [MHz]	6.48	7.58	7.59

Table 3 Averaged acoustic pressure of LGFUS according to diameter of CNT composite transducer.

N = 3 At Laser energy = 800 mJ	<b>2 cm</b>	<b>5 cm</b>	<b>8 cm</b>
<b>Peak P+</b>	32.60 ± 0.80	36.57 ± 1.1	53.50 ± 0.70
<b>Peak P-</b>	-9.53 ± 0.43	-17.96 ± 0.76	-25.24 ± 0.90

### 2.4.3 Relationship between Laser Energy and Acoustic Pressure

The correlation between laser energy and the resulting acoustic pressure is depicted in Figure 2.7 through a linear curve fitting. The pressure amplitudes at focal points were gauged across all excited laser energy levels in all three transducers of varying diameters (2 cm, 5 cm, and 8 cm). With increased laser energy (mJ/pulse), positive and negative pressures rose in all CNT-PDMS composite transducers (Tong et al., 2014). An exception was observed in the 2 cm diameter transducer, which demonstrated saturation at -10 MPa, with no further increase in negative pressure despite the rise in laser energy (Baac et al., 2015). Table 4 presents the values for the slopes, intercepts, and  $R^2$  of the linear fitting graphs in Figure 2.7. An  $R^2$  value closer to 1 indicates a strong linear correlation between the two values, except for the negative pressure curve for the 2 cm composite transducer.

Table 4  $R^2$ , intercept, and slope values for 2, 5, and 8 cm diameter of CNT composite transducers for both positive and negative pressure in Figure 2.7.

Diameter (cm)	Positive pressure			Negative pressure		
	$R^2$	Intercept	Slope	$R^2$	Intercept	Slope
2	<b>0.98</b>	19.45	0.019	0.71	-6.93	-0.004
5	<b>0.97</b>	10.26	0.033	0.92	-12.4	-0.007
8	<b>0.99</b>	1.039	0.066	0.94	-4.29	-0.029

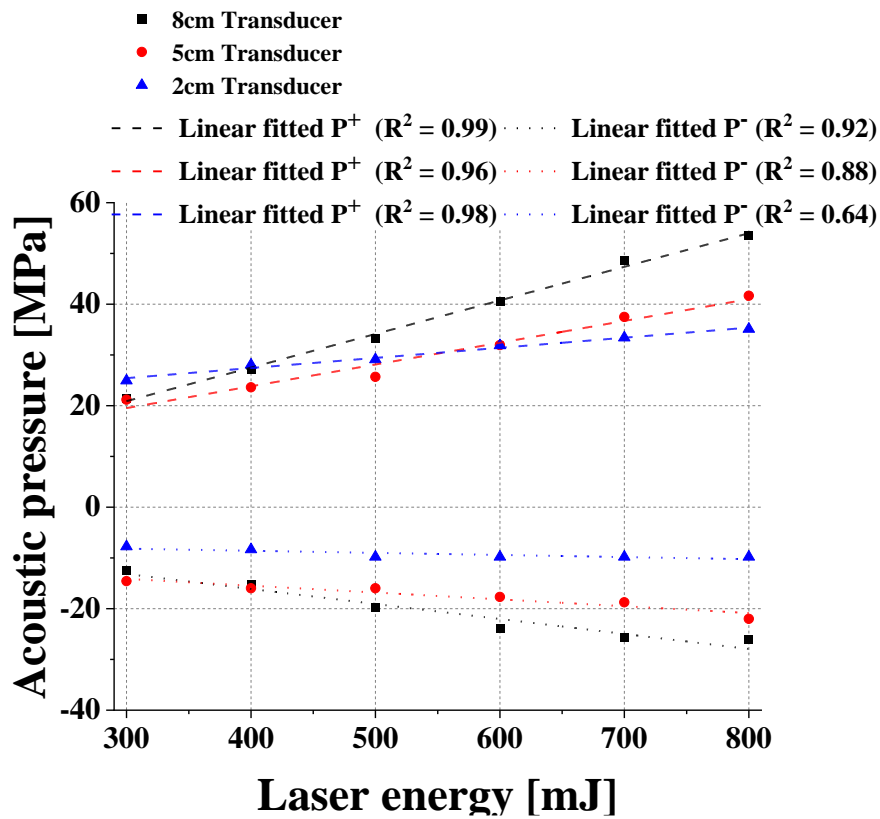


Figure 2.7 Linear curve fitting shows the relationship between laser energy and the acoustic pressure generated by CNT-PDMS composite transducers. It shows a linear relationship between laser energy and positive and negative acoustic pressures in all transducers, except the transducer with a 2 cm diameter. It shows saturation at -10 MPa in negative pressure with increased laser energy.

To confirm that LGFUS is output at sizes other than those used in the experiment, predictions were made using experimental values. Predictive acoustic pressure equations were calculated to predict the peak amplitude of LGFUS for CNT composite transducers from 2 to 8 cm in diameter at high laser energy levels above 700 - 800 mJ/pulse. The predicted peak positive and negative amplitudes for composite transducers between 2 cm and 8 cm were calculated by linear fitting of the measured values for laser energies at 700 mJ/pulse, and 800 mJ/pulse, as shown in Eq. (2.12) and (2.13). The calculated root mean square (RMS) errors of Eq. (2.12) and (2.13) are 1.7 MPa and 1.2 MPa, respectively:

$$\text{Predict } P^+ [\text{MPa}] = (0.00775 * E - 3.13) * D + 28 \quad (2.12)$$

$$\text{Predict } P^- [\text{MPa}] = (-0.00425 * E - 0.468) * D - 5.35 \quad (2.13)$$

(E = laser energy in mJ/pulse, D = diameter of transducer in cm.)

The predicted and measured peak amplitudes of the LGFUS are shown in Figure 2.8. The black and blue markers correspond to the predicted acoustic pressure. The measured acoustic pressure of the LGFUS is indicated as green and pink star markers. They show an agreement between the predicted and experimental values. For the 5 cm and 8 cm diameters, the measured values show a slight difference from the predicted values.

The acoustic pressure at the axial and lateral directions is shown in Figure 2.9. Ultrasonic decay is observed away from the focal point. Figure 2.9(d)–(f) shows the fall in the amplitude of the LGFUS away from the focal point.

A peak positive pressure of 20 MPa and peak negative pressure of -10 MPa were observed

at 0 mm with reference to the focal point (Figure 2.9d). When the needle hydrophone was moved along the y-axis, a peak positive acoustic pressure was observed to be  $\sim 20$ MPa, while a negative peak pressure was also observed to be  $\sim 10$  MPa at 0 mm at the focal point (Figure 2.9e). Furthermore, when the needle hydrophone was shifted along the z-axis, positive and negative peak pressures were measured to be  $\sim 20$  MPa and  $\sim 10$  MPa, respectively, at 0 mm with reference to the focal point (Figure 2.9f). The CNT-PDMS composite transducer used for these measurements was 2 cm in diameter. The LGFUS generated by the CNT composite transducer possesses a beam width of 2.1 mm in the axial direction and 0.60 mm in the lateral direction (Figure 2.9(d)-(f).)

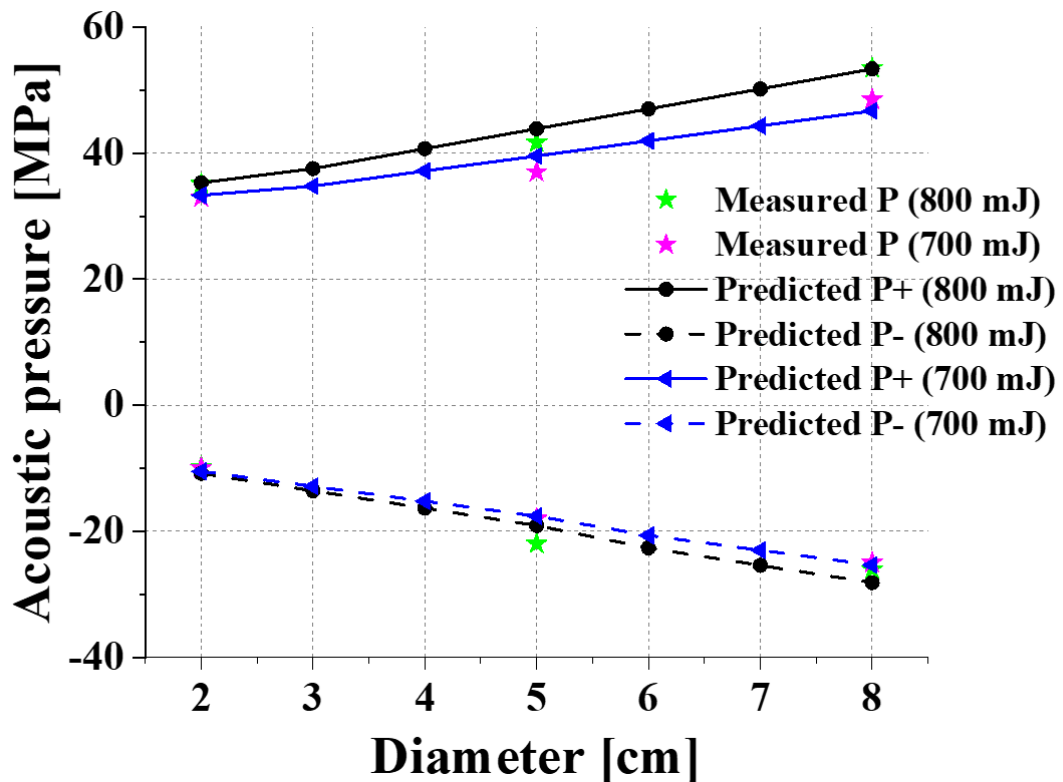
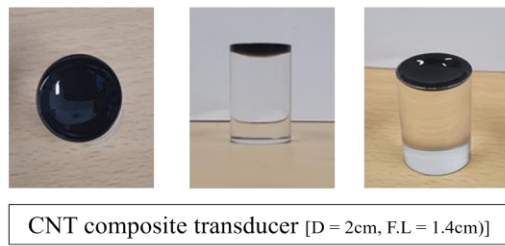
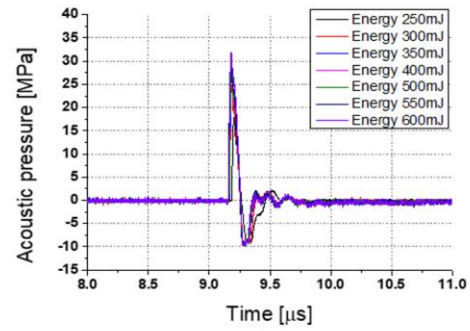


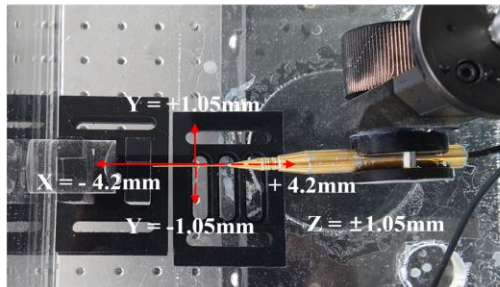
Figure 2.8 Scatter graph of predicted and experimental (measured) data of the CNT composite transducer for different diameters. The black circle and blue triangle marks correspond to the predicted values, while the green and pink star marks represent the measured values. This prediction was made at the laser energy of 700 mJ/pulse, and 800 mJ/pulse.



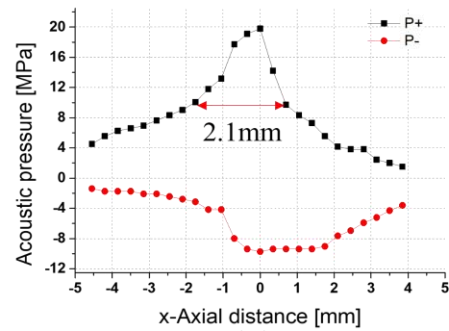
(a)



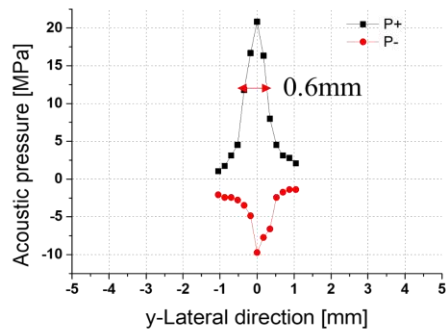
(b)



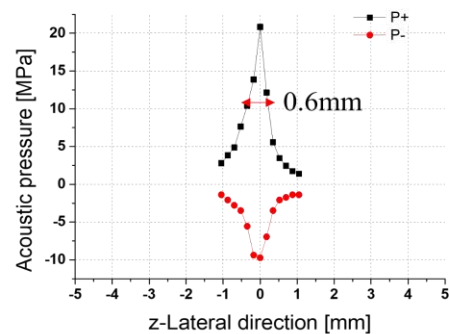
(c)



(d)



(e)



(f)

Figure 2.9 (a) CNT composite transducer of 2cm diameter. (b) LGFUS according to laser energy from CNT composite transducer of 2 cm diameter. (c) Experimental setup for measuring the focal point of the LGFUS. The focal point was at 0 mm. (d) The peak positive and negative pressures were observed at 0 mm concerning the focal point along the axial direction. (e) The peak pressures were observed at 0 mm regarding the focal point along the y-direction. (f) The peak pressures along the z-direction were also observed at 0 mm about the focal point.

## 2.5 Discussion

This study employed CNT composite transducers with an acrylic backing substrate and larger diameters for the experiments, successfully achieving higher peak amplitudes of LGFUS. The transducer with the acrylic backing generated the highest LGFUS compared with the ones with air and water. It was confirmed that the acoustic pressure was not sufficiently increased when the laser energy was irradiated, as water and air backing cannot support the expansion and contraction of PDMS. The CNT composite transducers demonstrated a consistent pattern of larger peak pressures with an increase in diameter. As the transducer's diameter expands, the laser energy dispersion also grows, leading to elevated peak pressures. Under identical laser energy conditions (800 mJ/pulse), the transducer with an 8 cm diameter produced the maximum positive and negative amplitudes of 53 MPa and -25 MPa, respectively. The peak pressures of LGFUS were increased with the increased input of laser energy. The high LGFUS amplitudes obtained in this study hold potential for use in various applications, such as transcranial studies, which were investigated in the following chapters.

The pattern of LGFUS was consistent across all three transducers. LGFUS exhibits a concise duration of 0.1~0.4  $\mu\text{s}$  (Lee, T. et al., 2018), in contrast to LGFUS originating from other sources (electrohydraulic, electromagnetic, and piezoelectric) (Xu et al., 2021, Cleveland and McAteer, 2012). The LGFUS observed in this study exhibited a duration of 0.2  $\mu\text{s}$  (Figure 2.6). A characteristic feature of the LGFUS, a broad frequency distribution, was observed within the frequency domain of the signals. As depicted in Figure 2.7, the frequency spectrum,

irrespective of transducer size, demonstrates a similar pattern with a center frequency and -6 dB bandwidth below 10 MHz. For smaller transducers of about 6 mm in size, the similar peak pressures were achieved, while they were at a higher main frequency of roughly 20 MHz (Baac et al., 2012). This is presumed to fluctuate based on the CNT composite transducer's manufacturing method and the laser system's characteristics.

Since LGFUS consists of high-frequency components, they attenuate more rapidly at high frequencies (Hsieh et al., 2015), which explains the faster decay of LGFUS. When the relationship between laser energy and different sizes of the composite transducer was analyzed, it was found that the measured peak pressures have a linear relationship with the laser energy. This finding confirms previous studies (Moon et al., 2017). However, for negative peak pressures, the 2 cm transducer reached saturation at higher laser energy levels (Baac et al., 2015) (Figure 2.7). We noted another significant phenomenon: the LGFUS generated from a 2 cm diameter transducer produces a higher sound pressure at a laser energy of 400 mJ than the LGFUS generated from transducers with 5 cm and 8 cm diameters. At a laser energy of 400 mJ, the 5 cm and 8 cm transducers exhibit nearly identical positive and negative pressures. Still, a divergence in peak pressures becomes evident as the laser energy is amplified. This confirms that the energy delivered to the CNT composite layer can vary with diameter, even when the same amount of laser energy is delivered per unit area. This implies that the maximum output can be more easily achieved at lower laser energies with a smaller transducer diameter. For future studies, we plan to conduct a quantitative evaluation of LGFUS energy

sources by calculating the energy per unit area of the delivered laser, considering the diameter of the transducer.

Figure 2.8 illustrates a correlation between the measured and predicted peak amplitudes of the LGFUS across various diameters of the CNT-PDMS composite transducers. The reference laser energy values for predicting peak amplitudes exceed 600 mJ/pulse. Higher energy values are typically utilized in an experimental setting since they have advantages for making predictions at these levels. For lower energy values, there is a negligible difference.

The comparison between the LGFUS signal of the CNT composite transducer and Extracorporeal Shock Wave Therapy (ESWT) reveals that the former has a narrower beam width than the latter. Conversely, the beam width of ESWT, as measured in (Gwan-Suk Kang, 2018), is 14 mm in the axial direction and 2 mm in the lateral direction (Figure 2.10(b)). This indicates that LGFUS through optoacoustic effects achieved a smaller focus than those generated through other sources including ESWT and TPS (ref.). The peak sound pressure of LGFUS was to be ~50 MPa. Although this output is less than the maximum sound pressure from the ESWT shock wave, which was 90 MPa, the 50 MPa sound pressure of LGFUS remains substantial. CNT composite transducers can alter the transducer and beam size with easier and more precise ways than other shock wave generators. However, one drawback is that the transducer is susceptible to damage from laser energy, necessitating improvements in durability. Even with its drawback, it appears significant to facilitate further applied research, such as neurostimulation or cell surgery.

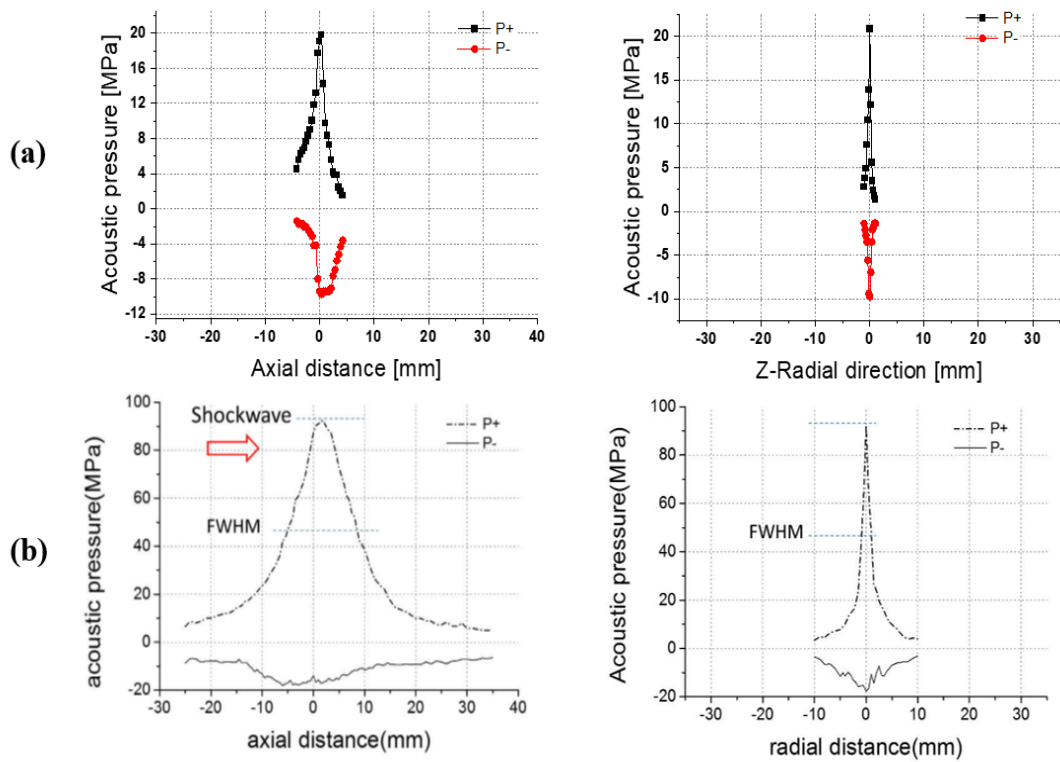


Figure 2.10 Comparison of pressure distribution from the geometric focus of LGFUS and ESWT along one-dimensional axial and radial directions. (a) Axial and Z-radial directions of LGFUS. (b) Axial and Z-radial directions of ESWT shock wave.

## 2.6 Conclusion

An experimental study was conducted to investigate the relationship between the composite transducer's diameter and the peak amplitude of LGFUS to fabricate a high-performance CNT composite transducer. For the experiments, composite transducers with larger diameters and acrylic substrates were used. The maximum diameter implemented in this study was 8 cm, which achieved a peak positive and negative pressure of 53 MPa and -25 MPa, respectively, at the focal point. Furthermore, the comparative analysis shows that the CNT composite transducer with a smaller diameter produced a narrower beam width at the focal point. The pressure of the LGFUS also demonstrated a linear relationship with the input laser energy. These results confirm that generating LGFUS through the optoacoustic method requires an optimal backing structure and transducer diameters. This understanding contributes to the technical advancement in constructing efficient optoacoustic transducers for optimal ultrasound generation.

# CHAPTER III

## APPLICATION OF LASER GENERATED FOCUSED ULTRASOUND

### 3.1 Applications of LGFUS

Shock waves were applied in brain applications, characterized by their wide frequency band and rapid rising time of a few nanoseconds. These shock waves particularly in lithotripsy have been employed to investigate the opening of the BBB of the rat (Kung et al., 2018). Additionally, the efficacy and stability of creating target lesions in the brain using histotripsy have been demonstrated (Van Lier et al., 2004).

LGFUS have shown potential in precision therapeutic ultrasound applications due to their ability to generate high-pressure, high-frequency shock waves with a focused spot. LGFUS generated by CNT composite transducers, despite having higher acoustic pressure compared to conventional ultrasound, generate short pulses lasting only a few nanoseconds like shock waves. This generates acoustic exposure in a confined area (Baac et al., 2012). LGFUS transducers have been utilized for high-precision therapies (Baac et al., 2013, Kim, J. et al., 2016). However, neurostimulation through shock waves generated by LGFUS remains an unexplored area. Their potential in neurostimulation has not yet been fully investigated.

This study aims to explore the feasibility of neurostimulation of the rat using LGFUS

produced by a CNT composite transducer. We recorded electroencephalography (EEG) signals in the brains of rats before, during, and after LGFUS stimulation, and compared them.

## **3.2 Method and Experimental Set up**

### **3.2.1 Animal Preparation**

This neurostimulation experiment was approved by the Jeju National University Institutional Animal Care and Use Committee (IACUC). All procedures and rat handling were performed following the ethical guidelines for animal studies. Rats were anesthetized intramuscularly during all procedures with a mixture of Zoletil 25 mg/kg (Virbac Laboratories, France) and Rumpun 4.6 mg/kg (Bayer, Leverkusen, Germany) and were monitored throughout the experiment. No pain or suffering was evident as a result of the procedure. A total of 5 male Sprague-Dawley rats (450g weight, Orient Bio Inc., Seongnam, Korea) were used in 2 experiments of this study. The hair on their heads was removed using a shaving razor and hair removal cream. The rats used in the experiment were euthanized by injecting CO<sub>2</sub> into an airtight container. The CNT composite transducer was fabricated by the method used in the study (Gisuk Kim et al., 2019))

### **3.2.2 EEG Signal Acquisition and Analysis**

EEG electrodes are positioned in consistent places based on the anatomy and size of the subject's head. Among the most popular layout conventions is the 10–20 International System (Jasper, 1958). The acquisition system utilized an OpenBCI Ganglion board, which permitted the recording of up to four EEG channels at 200 samples per second. In this study, the three

electrodes of the rat's head were placed at T5, T6, and the Reference region (Jiricek et al., 2021) and a ground electrode was placed on the ear. Data were acquired over Bluetooth using the OpenBCI GUI on a Windows 10 laptop (A. Ortuno, 2017). The range of noise was used to fit a 30<sup>th</sup>-order Blackman-window bandpass filter between 1–45 Hz for offline processing. A 1–60 Hz bandpass filter was used to remove overhead line noise during recording. The EEG channel with the lowest noise was calculated by finding the channel with minimal variance after bandpass filtering and removing the means. Then, the power spectrum of the EEG was calculated using a 1-second sliding window, with a 50% overlap with the prior window. Each one-second period was referred to as a single trial or epoch. The Welch's method was used to estimate the power spectrum.

The collected EEG data was examined in both time and frequency domains. In the time domain, we scrutinized the real-time EEG signals captured during the LGFUS stimulation. We also counted the peak signal over 6.7  $\mu\text{V}$  in the EEG signals before and after the LGFUS stimulation. The threshold for counting these peaks was established based on the standard deviation of the signal before stimulation. In the frequency domain, among the EEG bands, the theta (4-7 Hz) and alpha (8-12 Hz) bands, which are related to resting, breathing, and awareness training tasks (Van Lier et al., 2004, Frehlick et al., 2019, Vyazovskiy and Tobler, 2005), and a frequency band of 1–30 Hz, including most of the frequency band, were selected. Power spectral density (PSD) values in each theta, alpha, and 1–30 Hz frequency band before and after LGFUS stimulation were compared in the frequency domain.

### 3.2.3 Experimental Set up

The experimental setup performed in this study is shown in Figure 3.1. The locations of the EEG measurements are shown in Figure 3.1(a). EEG signals were measured at three points. The red circles indicate the EEG measurement positions and the green circle indicates the LGFUS stimulus location. The CNT composite transducer position of LGFUS stimulation was 3 mm left of the bregma in the rat brain. The brain stimulation area of LGFUS was the somatosensory cortex, which is positioned at 3 mm from the skull surface.

The EEG monitoring experiment was divided into two cases. In the first case, as depicted in Figure 3.1(b), to evaluate the feasibility of LGFUS stimulation, real-time EEG monitoring was performed in two rats. EEG signals were initially measured before the application of LGFUS, and their real-time responses were recorded as LGFUS was generated. The monitoring concluded 30 seconds after the termination of LGFUS stimulation. During this phase, we utilized laser energies of 300mJ and 350mJ with PRF of 1Hz and 2Hz, thereby enabling us to compare the EEG responses to varying energy levels and PRFs.

In the second case, to determine the effects of LGFUS stimulation, EEG signals were monitored before and after stimulation in three rats. To obtain reference data before stimulation, EEG signal response was measured for 10 min after anesthesia. Each rat was stimulated for 10 min. LGFUS accomplished stimulation from a CNT composite transducer driven by a laser pulse source. After stimulation, EEG signals were recorded for 20 minutes. For this experiment, we maintained the laser energy and PRF at a constant energy of 350mJ and 2Hz, respectively.

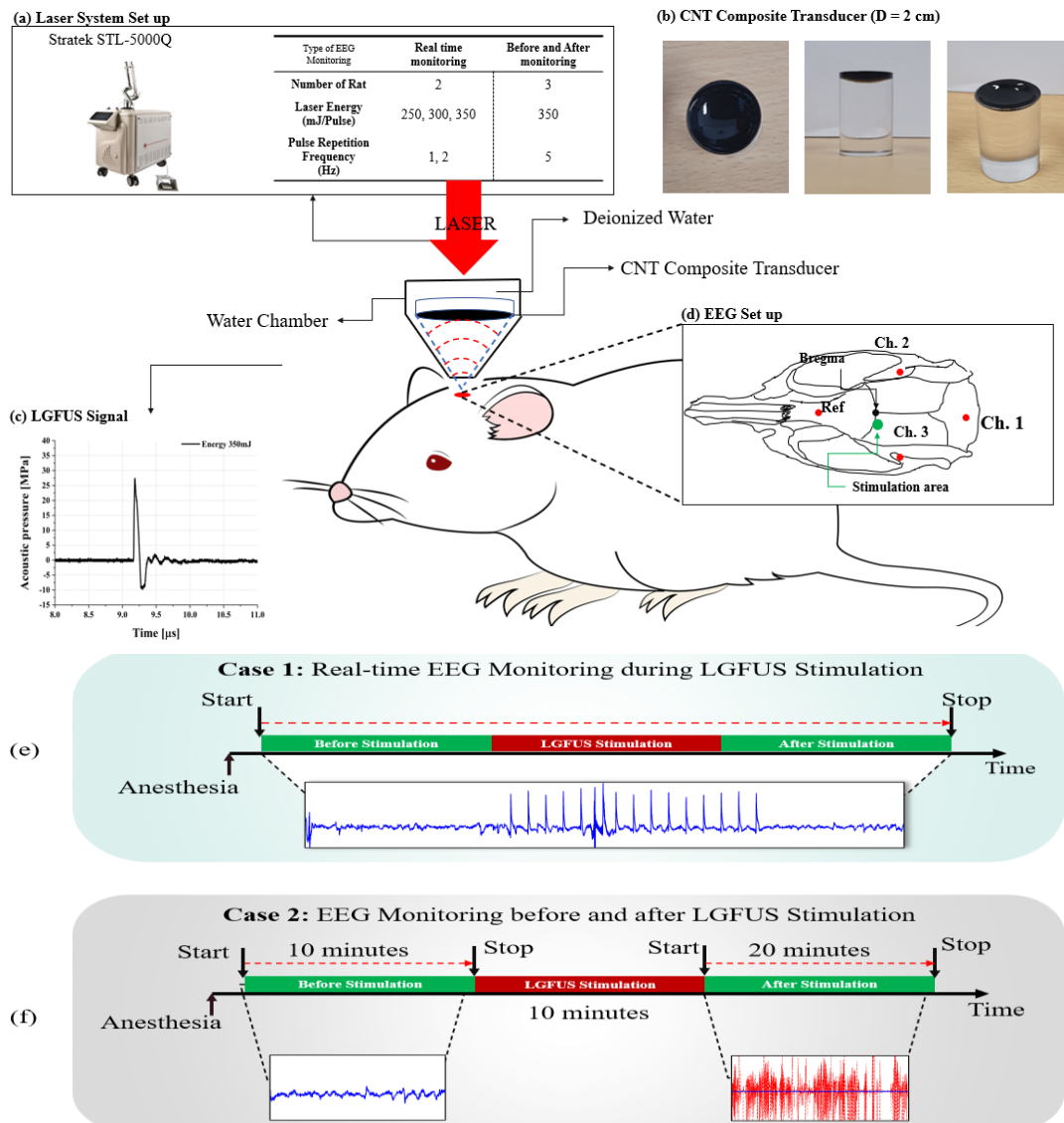


Figure 3.1 Experimental setup for measuring EEG signals upon brain stimulation of LGFUS generated by CNT composite transducers. (a) Information of Laser system and set up. (b) CNT composite transducer used in experiments. (c) LGFUS signal generated by CNT composite transducer. (d) EEG electrode set up. The Red circles is EEG measurement sites, green circle is targeting position of LGFUS. (e) Experimental sequence for real-time monitoring of EEG signals during brain stimulation by LGFUS. (f) EEG monitoring before and after LGFUS stimulation.

### 3.2.4 LGFUS Acquisition

The experimental setup is shown in Figure 3.2(a). When the laser was applied to the CNT composite transducer ( $F\# = 0.7$ , focal length = 1.4 cm) which was immersed in water, the CNT composite layer produced a LGFUS. A Q-switched Nd: YAG laser (STL-5000Q, Stratek, Anyang-si, Korea) with a wavelength of 532 nm and energy of 300mJ and 350 mJ was used to generate a LGFUS with a PRF of 1 to 2 Hz. The LGFUS generated by the CNT composite transducer has a beam width of 2.1 mm in the axial direction and 0.60 mm in the lateral direction (Figure 2.9). The pulse width of LGFUS is 200 ns in one cycle. A needle hydrophone (NH0200, Precision Acoustics Ltd, UK) was used to measure the shock pulse. The hydrophone was used with a 20 dB preamplifier (HP, Precision Acoustics Ltd, UK) powered by a DC coupler (Precision Acoustics Ltd, UK). The signal was monitored using an oscilloscope (LT354, Lecroy, New York, NY, USA). The peak positive and negative pressures of LGFUS are 27.3 MPa and  $-9$  MPa, respectively (Figure 3.2(b)). The center frequency is 4.3 MHz and  $-6$  dB bandwidth is 7 MHz, as shown in Figure 3.2(c).

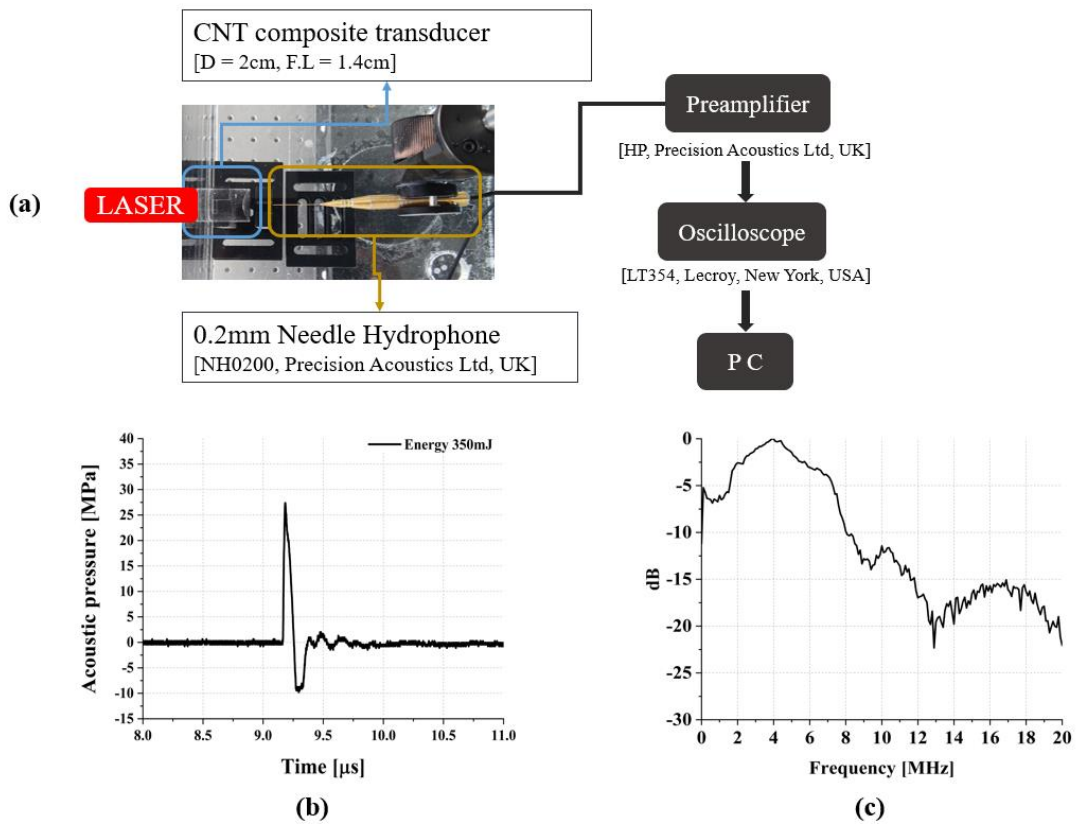


Figure 3.2 (a) Measurement set up for LGFUS from laser-generated by CNT composite transducer (Laser energy : 300 and 350 mJ, PRF : 1 and 2 Hz, Wavelength : 532 nm). (b) LGFUS signal and (c) Spectrum when laser energy is 350 mJ.

### 3.3 Results

#### 3.3.1 EEG Channel Selection

The EEG signals recorded across three channels were analyzed in the frequency domain. Figure 3.2 illustrates the disparities in EEG signals before and after LGFUS stimulation within the 1–30 Hz band for Rat 1. Table 5 displays the differences in PSD before and after stimulation for all rats across three bands, which includes the 1–30 Hz band, in 3 channels. The differences in EEG signals across the three channels before and after stimulation are distinctly presented. In channels 1 and 2, the PSD within the 1-30 Hz band was measured similarly. However, the PSD measured in channel 3 before and after stimulation was the lowest, yet the differential was the largest among the three channels. Table 1 shows the details of the differences in PSD before and after stimulation for all rats across three bands, including the 1–30 Hz band, for the three channels. Apart from channel 1 (theta and alpha bands) and channel 2 (alpha band) for Rat 2, the PSD post-stimulation was higher than that before stimulation. Areas exhibiting a clear difference of 15 dB, or more are shaded. Across all frequency bands for all rats, the shaded areas denote the most substantial differences in channel 3. Therefore, subsequent results were compared by selecting measurements exclusively from channel 3.

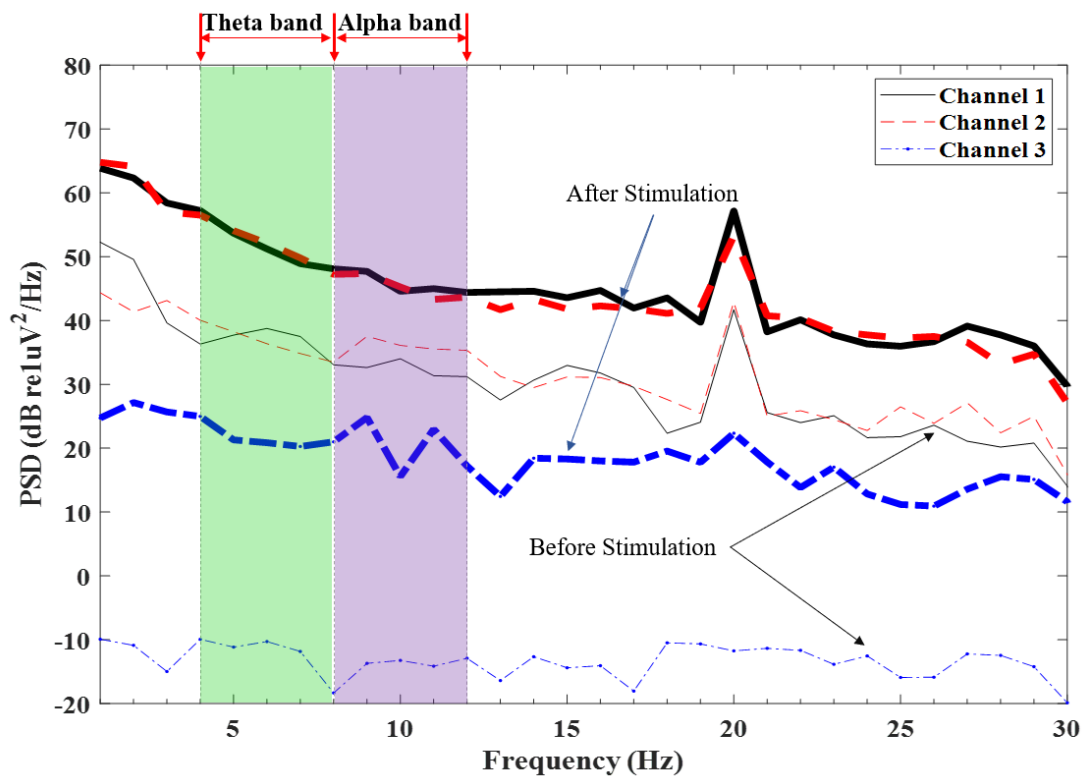


Figure 3.3 PSD comparison of 3 channels before and after LGFUS stimulation of EEG signals measured at Rat 1. The thick line is the PSD after stimulation, and the thin line is the PSD before stimulation.

Table 5 Difference in power before and after the LGFUS stimulation of 3 rats measured in 3 channels. Areas with a difference of 15 dB or more before and after stimulation are shaded;

$$\text{Power} = (\text{Integrated PSD}_{\text{AFTER}} - \text{Integrated PSD}_{\text{BEFORE}})/\text{Hz}$$

<b>Rat 1</b>	<b>CH.1</b>	<b>CH.2</b>	<b>CH.3</b>
<b>Theta band</b>	15.1	15.3	34
<b>Alpha band</b>	13.5	9.7	34.8
<b>1-30 Hz band</b>	14.6	13	31.7
<b>Rat 2</b>	<b>CH.1</b>	<b>CH.2</b>	<b>CH.3</b>
<b>Theta band</b>	-2.2	6	22.5
<b>Alpha band</b>	-3.7	-2.4	20.8
<b>1-30 Hz band</b>	3	7.7	17.6
<b>Rat 3</b>	<b>CH.1</b>	<b>CH.2</b>	<b>CH.3</b>
<b>Theta band</b>	5.6	33	19.5
<b>Alpha band</b>	6.3	32.2	15.9
<b>1-30 Hz band</b>	4.7	29.3	14.8

### 3.3.2 EEG Real Time Monitoring during LGFUS Brain Stimulation

The EEG signal resulting from LGFUS brain stimulation was segmented into real-time brain stimulation responses and time-domain comparisons of pre- and post-stimulation responses.

The responses in EEG signals, incited by real-time LGFUS stimulation in the rat brain, were explored and are depicted in Figure 3.4. Figure 3.4(a) displays real-time EEG signal alterations when the brain was subjected to LGFUS, produced with 300mJ laser energy and a PRF of 1Hz. It was verified that EEG signal peaks occurred at 1Hz intervals from the initiation of LGFUS stimulation and these peaks ceased upon termination of stimulation. The peak period observed in the EEG signal was found to coincide with the LGFUS stimulation period. Figure 3.4(b) validates the shift in the EEG signal peak during real-time brain stimulation, which was induced by an increase in the laser energy output to 350mJ. As the laser energy escalated, the size of the EEG signal peak generated by stimulation was also amplified, with the peak generation cycle measured at 1Hz. Figure 3.4(c) illustrates the peak variation in the EEG signal due to LGFUS brain stimulation generated at a lower laser energy of 300 mJ and an increased PRF of 2 Hz. As the laser energy and PRF were changed, the responses of the EEG signal from LGFUS stimulation also changed.

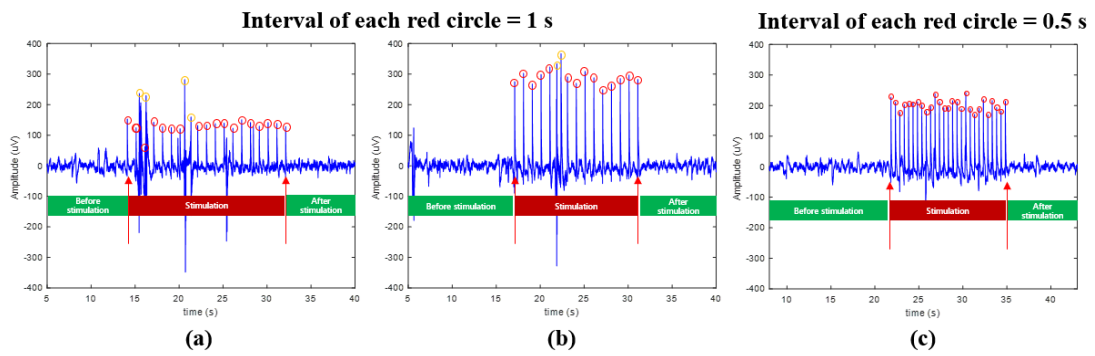


Figure 3.4 Real-time EEG signals generated by brain stimulation of LGFUS from CNT composite transducers. (a) EEG signal according to brain stimulation of LGFUS when laser energy is 300 mJ and PRF is 1 Hz. (b) Laser energy is 350 mJ and PRF is 1 Hz. (c) Laser energy is 350 mJ and PRF is 2 Hz.

Figure 3.5 compared the EEG signals of the LGFUS brain stimulation group with those of the sham control group. Figure 3.5(a) represented the EEG signal before LGFUS brain stimulation, exhibiting no discernable response apart from noise signals. Figure 3.5(b) displayed an EEG signal derived from real-time LGFUS brain stimulation, indicating that the peak signal coincided with the LGFUS stimulation PRF. Figure 3.5(c) illustrated an EEG signal recorded during a sham stimulation, in which LGFUS was not produced due to the prevention of laser energy transmission to the CNT composite transducer. Since the EEG signal captured during sham stimulation resembled the EEG signal before LGFUS stimulation, and alterations in the EEG signal were observed during real-time LGFUS brain stimulation.

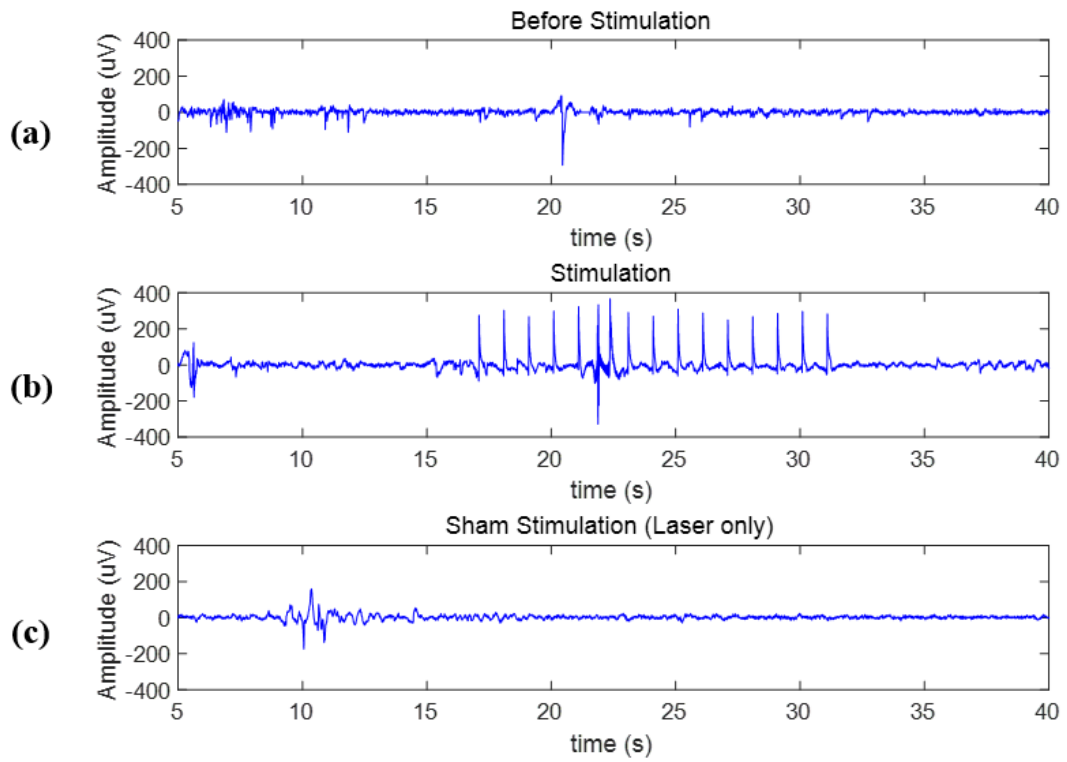


Figure 3.5 Comparison of EEG signals according to LGFUS stimulation conditions. (a) EEG signal before stimulation. (b) EEG signal upon real-time stimulation. (c) EEG signal upon stimulation with sham laser on without CNT composite transducer.

### 3.3.3 EEG Signal Before and After LGFUS Brain Stimulation

In the time domain, to measure the number of peaks under the influence of stimulation, the amplitude peaks with values higher than the standard deviation ( $\pm 6.7 \mu\text{V}$ ) were counted, as shown in Table II. It was confirmed that there were more peaks after LGFUS stimulation than before stimulation in all rats, although the differences in the number of peaks before and after LGFUS stimulation varied among the rats. Figure 3.6 shows the average number of peaks change before and after LGFUS stimulation by dividing the data according to time. The average number of peaks before and after each LGFUS stimulation was calculated by dividing the five minutes of data measured for each rat into 30 second intervals. The number of peaks observed post-stimulation in each rat was greater than those observed pre-stimulation. It was verified that for all rats, the disparity in the average peak counts within the middle data interval (from interval 4 to 7) both before and after stimulation was notably more significant than in other sections. However, in the case of Rat 2, the average number of peaks pre-stimulation exceeded those post-stimulation within the data intervals 1 to 3. Based on the results for data intervals 1 to 3 for Rat 2, it was established that the difference in the average peak count before and after stimulation over the entire duration was less pronounced for Rat 2 compared to the other rats.

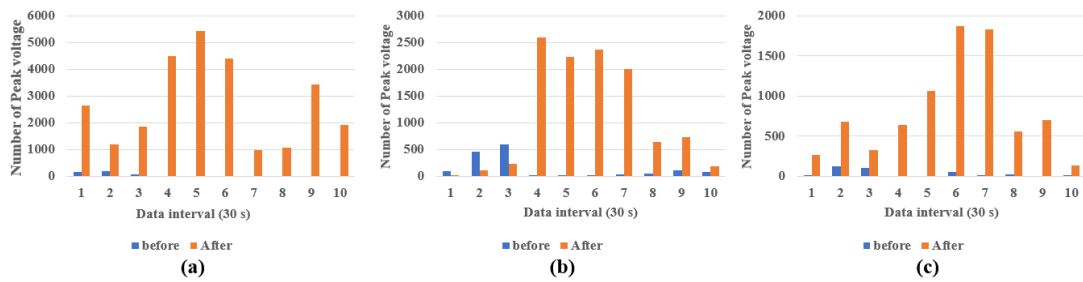


Figure 3.6 Total number of peaks at 30 s intervals before and after LGFUS stimulation of each rat. (a) number of peaks before and after stimulation for Rat 1, (b) Rat 2, and (c) Rat 3. The x-axis shows 5 minutes data divided into 10 sections with 30 second intervals, and the y-axis is the average number of peaks for each section.

In the frequency domain, Figure 3.7 shows the results of the EEG signal responses of three rats in the 1–30 Hz band before and after LGFUS stimulation. The EEG signal responses after stimulation were higher than those before in the range of 1–30 Hz. The differences between signal responses before and after stimulation were  $31.6 \pm 4.2$ ,  $14.7 \pm 11.0$ , and  $14.8 \pm 4.4$  dB for three rats. The PSD values of EEG signals measured before and after stimulation were distributed below and above 0 dB, respectively. Rat 1 had the most significant difference in PSD values among the three rats before and after stimulation, while Rat 3 had the smallest difference.

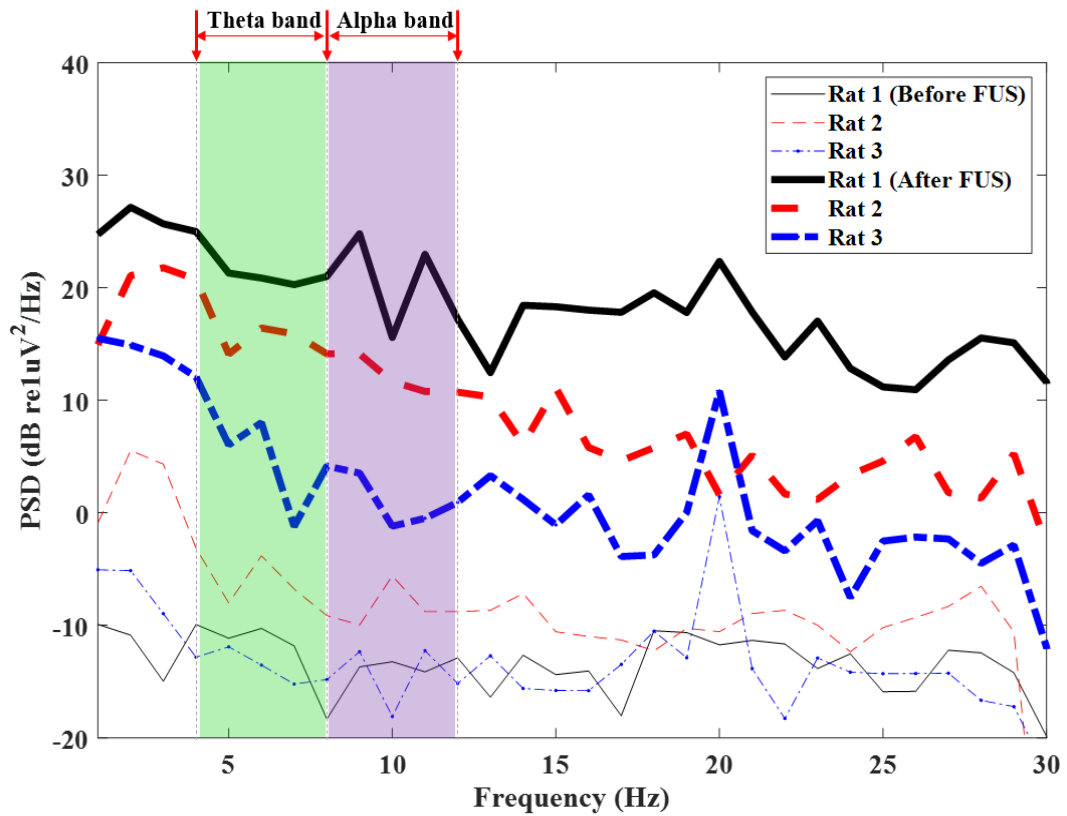


Figure 3.7 PSD of the EEG signal responses of 3 rats in 1-30 Hz band before and after LGFUS stimulation ( $p < 0.001$ ). The dotted line on the vertical axis indicates the PSD section in each theta band and the alpha band. The thick line is the PSD after stimulation, and the thin line is the PSD before stimulation.

The theta and alpha bands were extracted from the measured EEG signal responses shown in Figure 3.8 and the effects before and after LGFUS stimulation were compared. Figure 3.8(a) compares EEG signal responses in the theta band. The differences in EEG signal responses before and after stimulation for Rats 1, 2, and 3 were  $32.6 \pm 1.6$  dB,  $22.2 \pm 1.5$  dB, and  $19.6 \pm 4.7$  dB (ref  $1\mu\text{V}^2/\text{Hz}$ ), respectively. In Rats 2 and 3, the average difference in the theta bands before and after stimulation was lower than that of the alpha band. Figure 3.8(b) compares the PSD before and after stimulation in the alpha band. For Rat 1, the difference in PSD between before and after stimulation was  $34.7 \pm 4.9$  dB (ref  $1\mu\text{V}^2/\text{Hz}$ ). Rats 2 and 3 differed similarly,  $20.7 \pm 2.7$  dB and  $15.9 \pm 2.6$  dB (ref  $1\mu\text{V}^2/\text{Hz}$ ), respectively. In the other rat, the average difference in the overall theta band was similar to that in the alpha band. In channel 3 of Table 1, the dB differences before and after stimulation of the three rats at all frequency intervals were positive. In all frequency bands, there was a difference in magnitude in the order of Rats 1, 2, and 3. This result indicates that the magnitude of the signal increased after LGFUS stimulation.

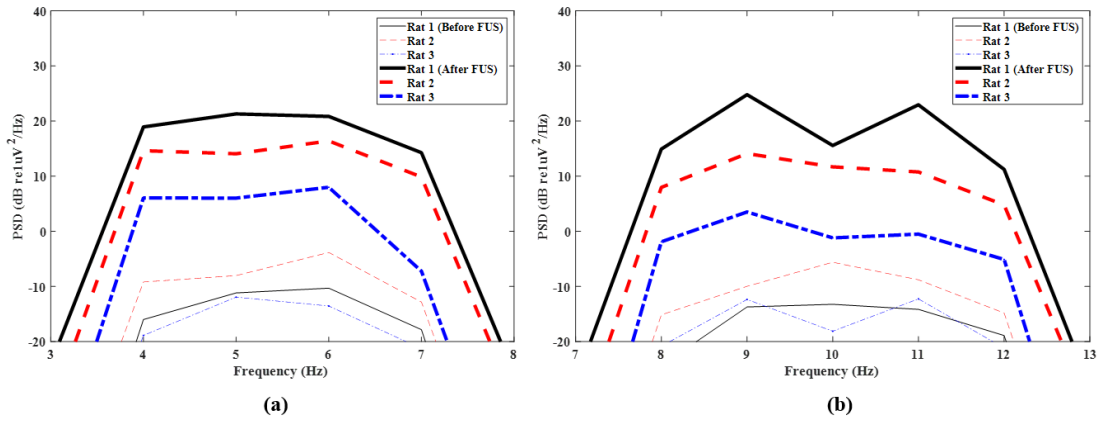


Figure 3.8 PSD of the EEG signal responses of 3 rats before and after LGFUS stimulation ( $p < 0.001$ ). (a) Theta(4-7 Hz) band. (b) Alpha (8-12 Hz) band. The thick line is the PSD after LGFUS stimulation, and the thin line is the PSD before LGFUS stimulation.

Additional experiments were conducted to verify the recovery of the increased EEG signal after LGFUS brain stimulation, as shown in Figure 3.9. Figure 3.9(a) outlines a procedure that compares the EEG signal recorded during LGFUS stimulation, the signal measured after stimulation, and the EEG signal 30 minutes after stimulation to verify the recovery of the EEG signal. The EEG signals before, after, and during brain stimulation were analyzed with a spectrogram, shown in Figure 3.9(b). The spectrogram before stimulation was devoid of any signal except noise and showed continuous intensity changes during stimulation. After stimulation, the change in intensity decreased compared to the results during stimulation. Still, it continued to be observed, and after 30 minutes of stimulation, it showed a similar level to the results before stimulation. Figure 3.9(c) shows the EEG signals before and after LGFUS brain stimulation and the signals during stimulation. The highest EEG signal was observed during LGFUS stimulation, and the EEG signal decreased by more than 10 dB after stimulation. EEG signals were also measured 30 minutes after LGFUS stimulation was completed, as shown in Figure 3.9(d). It was confirmed that the EEG signal measured 30 minutes after stimulation had decreased to a level almost equal to the pre-stimulation EEG signal.

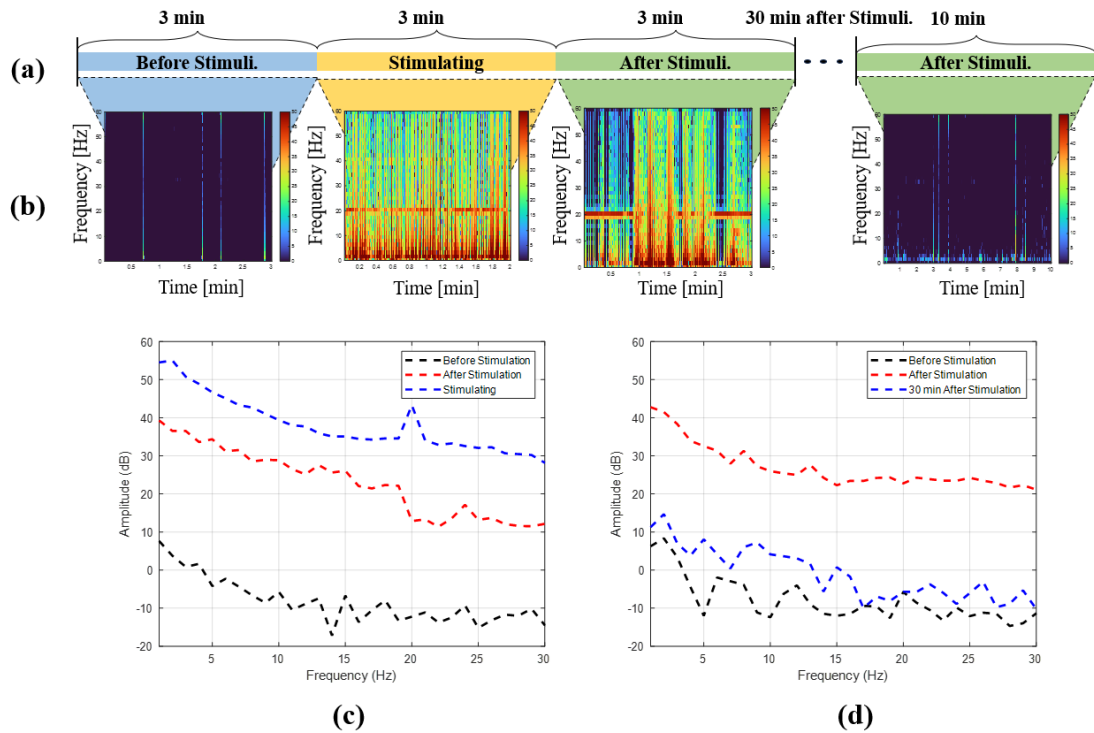


Figure 3.9 Comparison of the increased EEG signal after LGFUS stimulation and the recovered EEG signal 30 minutes after stimulation. (a) EEG signal measurement setup from before LGFUS stimulation to 30 minutes after stimulation. (b) Spectrogram of EEG signal according to brain stimulation of LGFUS for each experimental part. (c) Comparison was made of the EEG signals measured before and immediately after LGFUS stimulation with those measured during real-time stimulation. (d) Comparison was made of the EEG signals before, immediately after, and 30 minutes after LGFUS stimulation.

### 3.4 Discussion

This study is a preliminary study to confirm the feasibility of brain stimulation with LGFUS generated from CNT composite transducers. We measured and compared EEG signals from the rat brains before, during, and after stimulation by LGFUS generated by a CNT composite transducer. As a result of real-time EEG monitoring during brain stimulation by LGFUS, it was confirmed that the EEG response changed due to the influence of LGFUS. In the time domain, the number of peaks of EEG signals after LGFUS stimulation of all three rats was significantly higher than before stimulation. In the frequency domain, three rats showed differences in PSD and RMS values before and after LGFUS stimulation ( $p < 0.001$ ) in three frequency bands: alpha, theta, and 1–30 Hz. These differences in EEG signals before, during, and after LGFUS stimulation of the three rats are mainly due to the effect of LGFUS. Therefore, the feasibility of brain stimulation was confirmed by the characteristics of the LGFUS generated by the CNT composite transducer, and to the best of our knowledge, this is the first study to be attempted.

The intensity of ultrasound used for conventional neurostimulation is usually over  $3.0 \text{ W/cm}^2$  (Kim, H. et al., 2014) and the pulse duration is 20 ms to 320 ms (King et al., 2013), using various parameters. In a previous study, the intensity range without tissue damage was  $2.5\text{--}2.8 \text{ W/cm}^2$  ( $I_{\text{spta}}$ ) (King et al., 2013). The intensity ( $I_{\text{spta}}$ ) of the LGFUS used in this study was  $8 \text{ mW/cm}^2$  ( $I_{\text{sptp}} = 68 \text{ kW/cm}^2$ ,  $I_{\text{sppa}} = 10.7 \text{ kW/cm}^2$ ), smaller than that used in a previous study. In addition, there was no histological damage at the sound pressure of the

LGFUS without cavitation ( $-9.79$  MPa) (Kung et al., 2018, Lin et al., 2014).

Boiling histotripsy has a negative pressure of 10–20 MPa and a positive pressure of 70 MPa or more (Khokhlova et al., 2017). In addition, the duty cycle of the LGFUS is very low, and the peak positive pressure of the LGFUS used in this study is 30 MPa, and the negative pressure is  $-9$  MPa. Therefore, it has characteristics suitable for in vivo applications that prevent ultrasound heating of biological tissue. Tissue damage may occur because of the high peak sound pressure of the LGFUS from the CNT composite transducer. The degree of damage varies depending on the number of cycle pulses (Xu et al., 2021), sound pressure level, and sonication times (Kung et al., 2018, Xu et al., 2021). The physical damage to tissues by ultrasound is mainly caused by cavitation. For shock-scattering histotripsy, shock waves of 3–10 cycle pulses were used. Positive pressure ( $>50$  MPa) and negative pressure ( $-15$  to 25 MPa) (Xu et al., 2021) at much higher levels than the acoustic pressure used in this study were used. An autopsy of the rat brains after stimulation with LGFUS confirmed no apparent damage, as shown in Figure 3.10. Additionally, brain sections were stained hematoxylin and eosin (H&E) to observe damage caused by LGFUS brain stimulation as shown in Figure 3.11. It was confirmed that no damage was shown in the H&E staining by LGFUS. This study demonstrated the feasibility of brain stimulation through LGFUS, which is different from conventional ultrasound. When the intensity of the LGFUS from the CNT composite transducer is compared with other similar studies as a quantitative value, it can be sufficiently predicted that there will be no brain tissue damage. In future experiments, the degree of

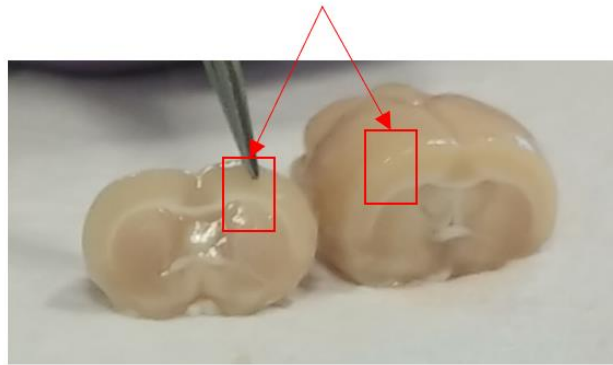
damage will be derived through quantitative evaluation while controlling the parameters of the LGFUS stimulation measured in three channels before and after LGFUS stimulation for all rats.

### Stimulation Area



(a)

### Stimulation Area



(b)

Figure 3.10 Autopsy rat brain after LGFUS brain stimulation. (a) LGFUS stimulation area in the rat brain (b) Brain slice of the LGFUS stimulation area.

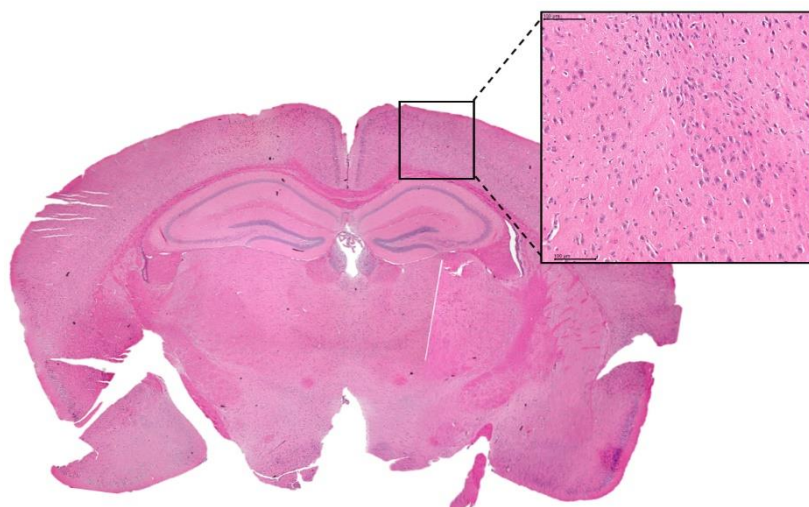


Figure 3.11 H&E-stained brain sections after LGFUS exposure for 3 minutes.

EEG signals before and after LGFUS stimulation were measured in three channels for all rats. The more significant difference in EEG signals in channel 3 before and after LGFUS stimulation may be due to the stimulation position of the primary somatosensory cortex. Local stimulation to this primary somatosensory cortex propagates to the contralateral body, which may have a smaller response to EEG signals in another channel. However, this study was designed as a trial to measure the EEG response by LGFUS stimulation in the rat brain using a CNT composite transducer with precision targeting. As a future study, the response according to each EEG channel has to be confirmed and analyzed by a CNT composite transducer's precision target by LGFUS.

The results based on the standard deviation of the EEG signals among the three rats before LGFUS stimulation in the raw data have the advantage of directly confirming EEG changes due to LGFUS stimulation. In Rats 1, 2, and 3, the differences in the number of peaks before and after LGFUS stimulation were calculated to be approximately 41, 1.6, and 14.9, respectively. Rat 2 had the highest number of EEG signal peaks before LGFUS stimulation and the lowest number after stimulation. Although each rat showed a difference in the number of EEG peaks before and after LGFUS stimulation, the degree of difference in the number of peaks among the rats varied. This is expected from the individual differences in each rat. Further studies are needed to elucidate the cause of this variation. In this experiment, the number of rats used as an experiment to confirm the brain stimulation effect of LGFUS from CNT composite transducers was insufficient to derive statistical significance. However, the

results of the stimulation of the brains of five rats confirmed that changes in EEG signals occur after LGFUS stimulation. In future experiments, the brain stimulation effect of the LGFUS can be confirmed by increasing the number of experimental animals to obtain statistical results.

To validate that the changes in the rat's EEG signal were due to LGFUS brain stimulation, both the EEG signal during sham stimulation and the EEG signal in response to shifts in the LGFUS stimulation location were investigated. First, EEG signals from the sham control group were measured when the laser was generated without a CNT composite transducer, so it could be confirmed that it was not affected by the laser light. Moreover, there was no real-time EEG signal response when an externally loud sound was played on the rats. Therefore, the EEG signals were not from the auditory stimulation through the ears. Secondly, the amplitude of EEG signals was examined when the focal point of the LGFUS was shifted from the brain surface to the cortical bone. This was carried out to validate the alterations observed due to LGFUS stimulation. The EEG signal was confirmed to vary by the stimulation cycle (1 Hz) of the LGFUS, as shown in Figure 3.12(a). When the focus of the LGFUS was directed to the rat's cortical bone, no change was detected in the EEG signal during the stimulation cycle, as depicted in Figure 3.12(b). Consequently, it was ascertained that the brain stimulation by LGFUS modified the characteristics of the rat's EEG. However quantitative assessment is required through specific stimulation evaluation by examining neuronal activation, calcium channel response, and changes in cell stimulation to evaluate the efficacy of very short pulses

of brain stimulation.

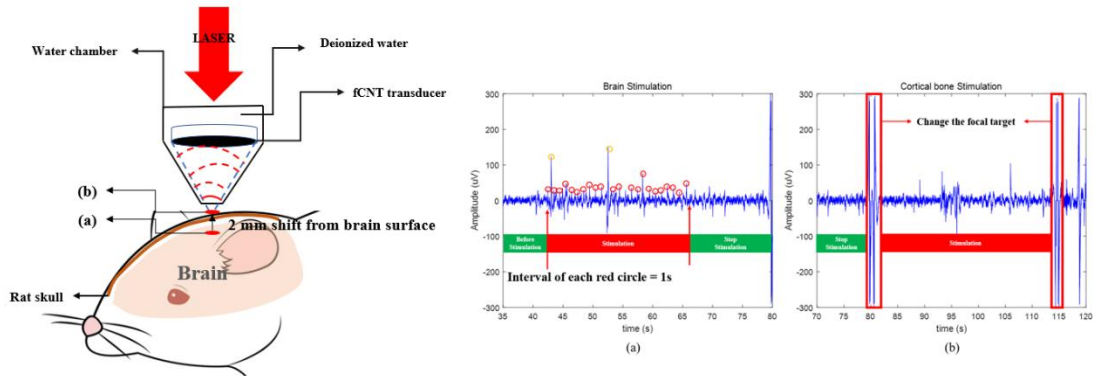


Figure 3.12 Real-time EEG signal change with respect to the focal position of the LGFUS. (a)

EEG signal with the LGFUS focus shifted to the rat's brain surface at 250 mJ of laser energy

and 1 Hz of PRF. (b) EEG signal with the focus of the LGFUS shifted to the rat's cortical bone.

### **3.5 Conclusion**

We stimulated rat brains using LGFUS generated by a CNT composite transducer. We observed changes in the theta, alpha, and 1–30 Hz bands of the EEG signals before, during, and after LGFUS. This method enables stimulation of a very small target area, providing a means for precise verification of brain function. The high spatial resolution of LGFUS makes it possible for the stimulation of specific brain regions, adjusting the location and depth within the brain.

## **Chapter IV**

# **PRELIMINARY EXPERIMENT TO EXPLORE THE CHARACTERISTICS OF LGFUS THROUGH HUMAN SKULL CADAVER**

### **4.1 Introduction**

The human skull presents a challenge for ultrasound transmission due to its complex heterogeneous composition of solid, multilayered, fluid-filled, and porous tissues. Nevertheless, ultrasound remains an attractive therapeutic tool because of its noninvasiveness and nonionization. FUS has been proposed to treat conditions such as essential tremor (Kalia et al., 2013), brain tumors (Fry, 1977, Hynynen and Jolesz, 1998, Tanter et al., 1998, Tobias et al., 1987) and stroke (Kalia et al., 2013) for targeted antibody delivery (Brighi et al., 2020). FUS produces thermal ablation of target tissue while sparing surrounding structures by concentrating energy in a small focal region. The main challenge in the use of FUS for brain therapy is to compensate for the attenuation and diffraction effects caused by the bone of the skull. The skull bone has a higher speed of sound in the longitudinal direction and a higher density than the soft tissue. The skull's absorption of ultrasound energy causes heating, and when combined with the skull's complex morphology, effectively focusing ultrasound becomes challenging (Hynynen and Jolesz, 1998, White et al., 1968, Clement et al., 2001,

Pichardo and Hynynen, 2007).

The FUS generated by a single transducer is often subject to significant distortion and attenuation due to the dense and complex structure of the skull. The length of the signal after penetrating the skull is extended compared to its original length before penetration. For effective brain stimulation, it is critical to achieve precise targeting within the brain after penetration of the skull. However, the distortion that occurs as the signal travels through the skull can alter the beam size, compromising targeting accuracy. Compared with the conventional FUS techniques, LGFUS is characterized by its ability to form a small focus, and future research may enable more precise targeting if focus correction is performed by substrate shape or lens. The primary focus of LGFUS research has been to verify the responses elicited by direct stimulation of neurons, cells, and tissues. However, fewer studies have been devoted to verifying the skull penetration of LGFUS or characterizing the altered signal after skull penetration. Therefore, it is imperative to determine whether LGFUS can effectively penetrate the skull. This step is critical in the pursuit of using LGFUS for therapeutic purposes, such as non-invasive treatment of neurological disorders, where precise targeting and minimal distortion of the ultrasound beam are critical to success.

The purpose of this study is to investigate the changes in ultrasound signal characteristics after penetration of a human skull cadaver using LGFUS and to evaluate the potential of this technology. LGFUS has several important advantages, especially when dealing with the challenge of skull penetration. One significant advantage is the ability to generate very short

pulse widths. The ability to produce such short pulses allows for more precise targeting, concentrating the ultrasound waves on a specific area with greater accuracy. This can potentially improve the safety and efficacy of treatments that rely on precise targeting of specific brain regions, such as tumor ablation or targeted drug delivery.

## 4.2 Material and Experimental Set up

### 4.2.1 Skull Acquisition

The skull cadaver provided by Jeju National University Medical School was approved by the Institutional Review Board (IRB) of Jeju National University Hospital. Experiments were conducted to investigate the LGFUS characteristics after penetration of skull cadavers.

### 4.2.2 Morphological Information and Experimental Set up

CT images were collected to determine measurements of density, sound speed, and thickness. The density and sound speed of the skull were calculated from the Hounsfield Unit (HU) values, a unit that signifies the radiodensity in CT imaging. The HU values at the measurement location were extracted ten times and averaged to compute the density and sound speed of the transducer's insonating area from the CT data. The skull density was calculated by substituting the extracted HU value into Eq. (4.1). The maximum and minimum HU values were 2400 and 1024, respectively (Marsac et al., 2017).

$$\rho = \rho_{min} + (\rho_{max} - \rho_{min}) \frac{HU - HU_{min}}{HU_{max} - HU_{min}} \quad (4.1)$$

The sound speed of the skull was computed as a linear function of density by substituting the calculated density from Eq. (4.1) into Eq. (4.2).

$$C = C_{min} + (C_{max} - C_{min}) \frac{\rho - \rho_{min}}{\rho_{max} - \rho_{min}} \quad (4.2)$$

The minimum and maximum speeds of sound ( $C_{\min}$  and  $C_{\max}$ ) are presumed to be 1500 and 4000 m/s, respectively. In summary, the density and sound speed of the skull are derived from the HU values. The average skull density, sound speed, and thickness is  $1995 \pm 52.6$  kg/m<sup>3</sup>,  $2963.8 \pm 63$  m/s and  $5.56 \pm 0.5$  mm, respectively, as shown in Figure 4.1(a).

The experimental setup is shown in Figure 4.1(b). When the laser was applied to the focused CNT composite transducer (Diameter = 50 mm, Focal length = 50 mm) immersed in the water. A pulse laser system (Tribeam, Jeisys, Medical Inc, Seoul, Korea) with a wavelength of 532 nm and energy of 200 mJ was used to generate the LGFUS with a pulse repetition frequency of 1 Hz. A needle hydrophone (TNU001A, Onda, Sunnyvale, CA, USA) was used to measure the LGFUS transmitted through the center of skull. The hydrophone was used with a 30 dB preamplifier (HPA30, Onda, Sunnyvale, CA, USA) powered by a 15V power supply (E3631A, Agilent, Santa Clara, CA, USA). The signal was monitored with an oscilloscope (LT354, Lecroy, New York, USA).

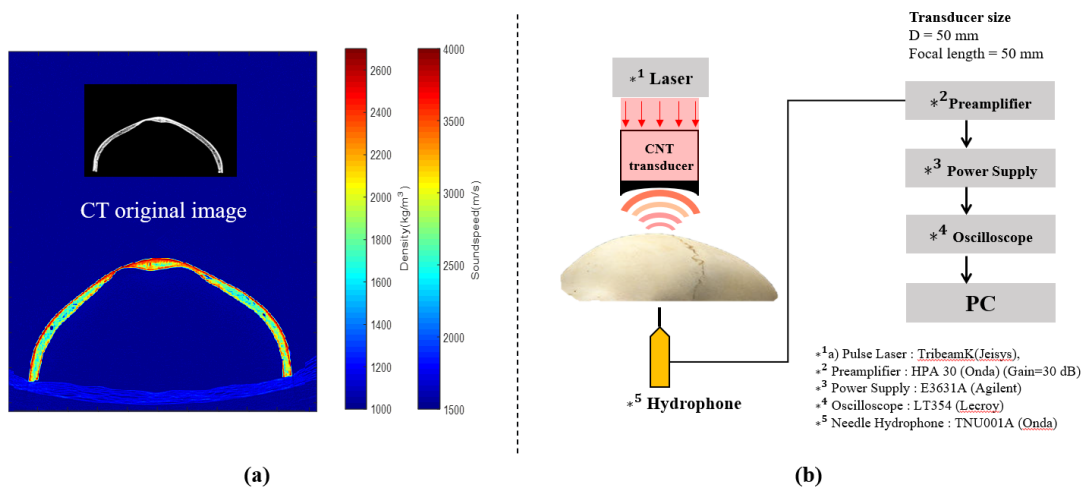


Figure 4.1(a) Sound speed and density distribution extracted from CT images of the center of the skull cadaver. (b) Measurement setup before and after skull penetration of LGFUS generated from a CNT composite transducer.

## 4.3 Results

### 4.3.1 Characterization of LGFUS with and without Skull Cadaver

The LGFUS signal from the CNT composite transducer without the skull cadaver has a short rise time of 0.1  $\mu\text{s}$  and the pulse duration of an LGFUS is 2  $\mu\text{s}$  including the negative pressure (Figure 4.2(a)). The maximum positive and negative pressures of the measured signal are 14.6 MPa and 11.66 MPa, respectively. The center frequency of the signal is 1 MHz and the -6 dB frequency bandwidth is 2.15 MHz Figure 4.2(b). Figure 4.2(c) shows the measured signal after transmission through the cadaver. The maximum positive and negative pressures decreased by 1.1 MPa and -1.1 MPa, respectively. The pulse duration increased to 4.3  $\mu\text{s}$ . The rise time of the signal was 0.78  $\mu\text{s}$ , the center frequency was 464 kHz, and the -6 dB frequency bandwidth was 1.34 MHz. Results are shown in Table 3 to compare the characteristics of LGFUS with and without skull cadaver penetration. Without the skull cadaver, the focal point of LGFUS was determined to be 51.5 mm. However, with skull cadaver penetration, the focal point was observed to shift forward to 39.3mm, as shown in Figure 4.3.

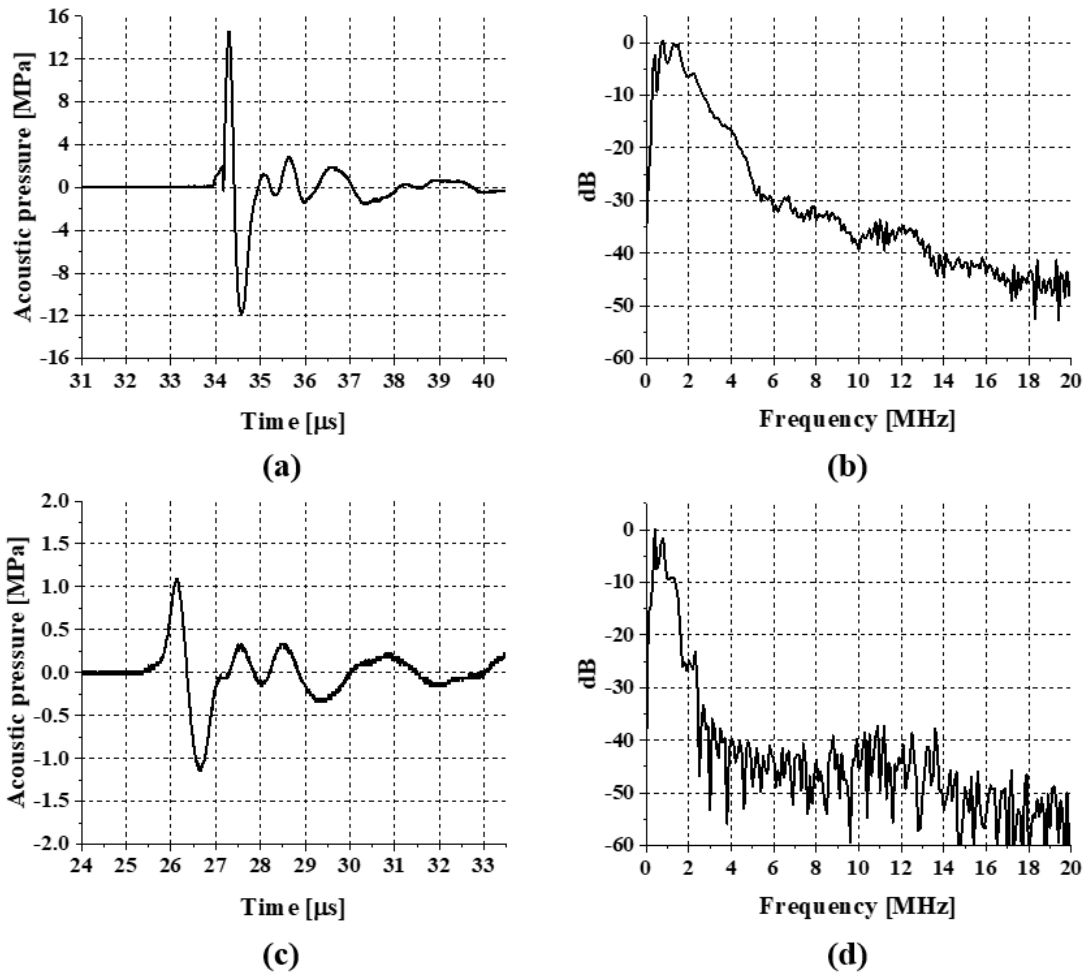


Figure 4.2 The signal generated by the CNT composite transducer before and after LGFUS penetration into the human skull cadaver. (a) LGFUS measured before cadaver penetration, (b) spectrum. (c) LGFUS measured after human skull cadaver penetration, (d) spectrum.

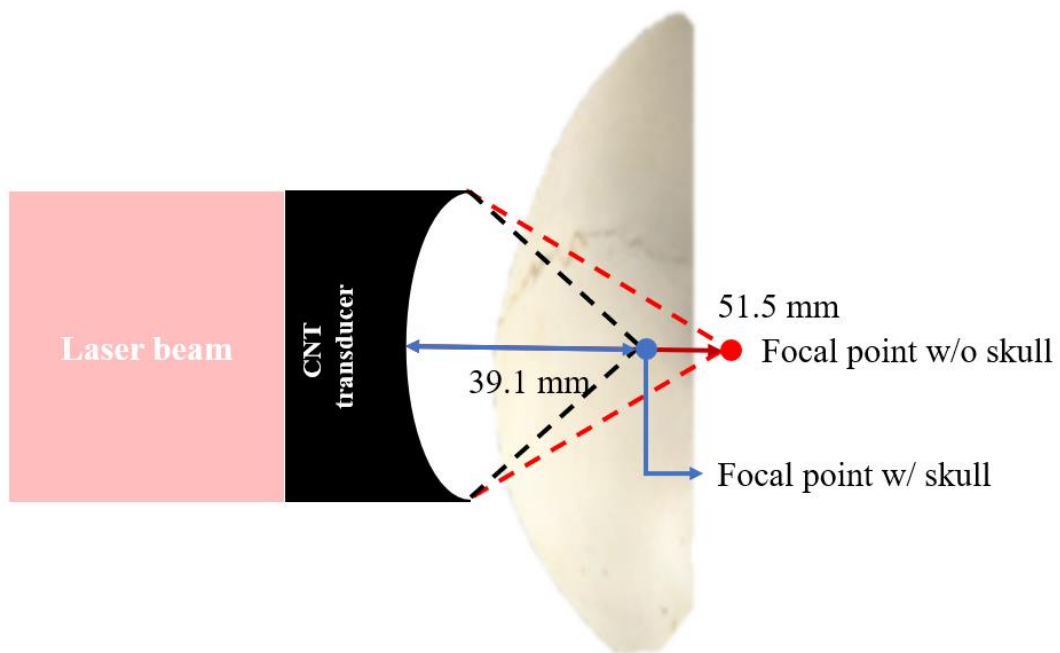


Figure 4.3 The focal position of LGFUS changes during human skull cadaver penetration.

Table 6 Characteristics of LGFUS with and without human skull cadaver penetration

	Acoustic Pressure [MPa]	Pulse Duration [ $\mu$ s]	Focal point Position [mm]	Center Frequency [MHz]	-6dB Bandwidth [MHz]
<b>Without skull</b>	14.6 -11.66	2	51.5	1	2.15
<b>With skull</b>	1.1 -1.1	4.3	39.1	0.464	1.34

### 4.3.2 Comparison of HIFU and LGFUS with and without Skull Cadaver Penetration

A comparison was made between the signals before and after skull cadaver penetration from LGFUS and HIFU skull cadaver penetration signals. The properties of HIFU and LGFUS produced by the CNT composite transducers, both initial and improved, were examined after penetrating the skull cadaver, as shown in Figure 4.4. These results are illustrated in Figure 4.4(a), which shows the LGFUS signals from the initial CNT composite transducer fluctuating with and without skull cadaver penetration. Acoustic pressure was measured at 332 kPa before penetrating the skull cadaver, and at 22 kPa after penetrating, resulting in a penetration rate of 6.6%. The pulse duration increased from 3.6  $\mu\text{s}$  before penetration to 9  $\mu\text{s}$  post-penetration. The developed CNT composite transducer generated LGFUS observed a penetration rate of 7.5%, with acoustic pressures varying from 14.6 MPa to 1.1 MPa depending on skull cadaver penetration. The output intensity was increased even though the penetration rate was similar to the initial transducer. The pulse duration increased by 3.9  $\mu\text{s}$ , from 4.5  $\mu\text{s}$  to 8.4  $\mu\text{s}$ , as shown in Figure 4.4(b). Figure 4.4(c) displays the signal characteristics generated from the HIFU transducer before and after skull penetration, with sound pressure and pulse duration settings like the LGFUS characteristics. Therefore, the results suggest that skull cadaver penetration alters the signal characteristics of HIFU, changing the pulse duration and output intensity. The pulse duration increased from 4 to 7  $\mu\text{s}$ , while the acoustic pressure decreased from 230 kPa to 15 kPa, resulting in a penetration rate of 6.5%. All three signals showed similar penetration

rates with the CNT composite transducer displaying the highest rate at 7.5%.

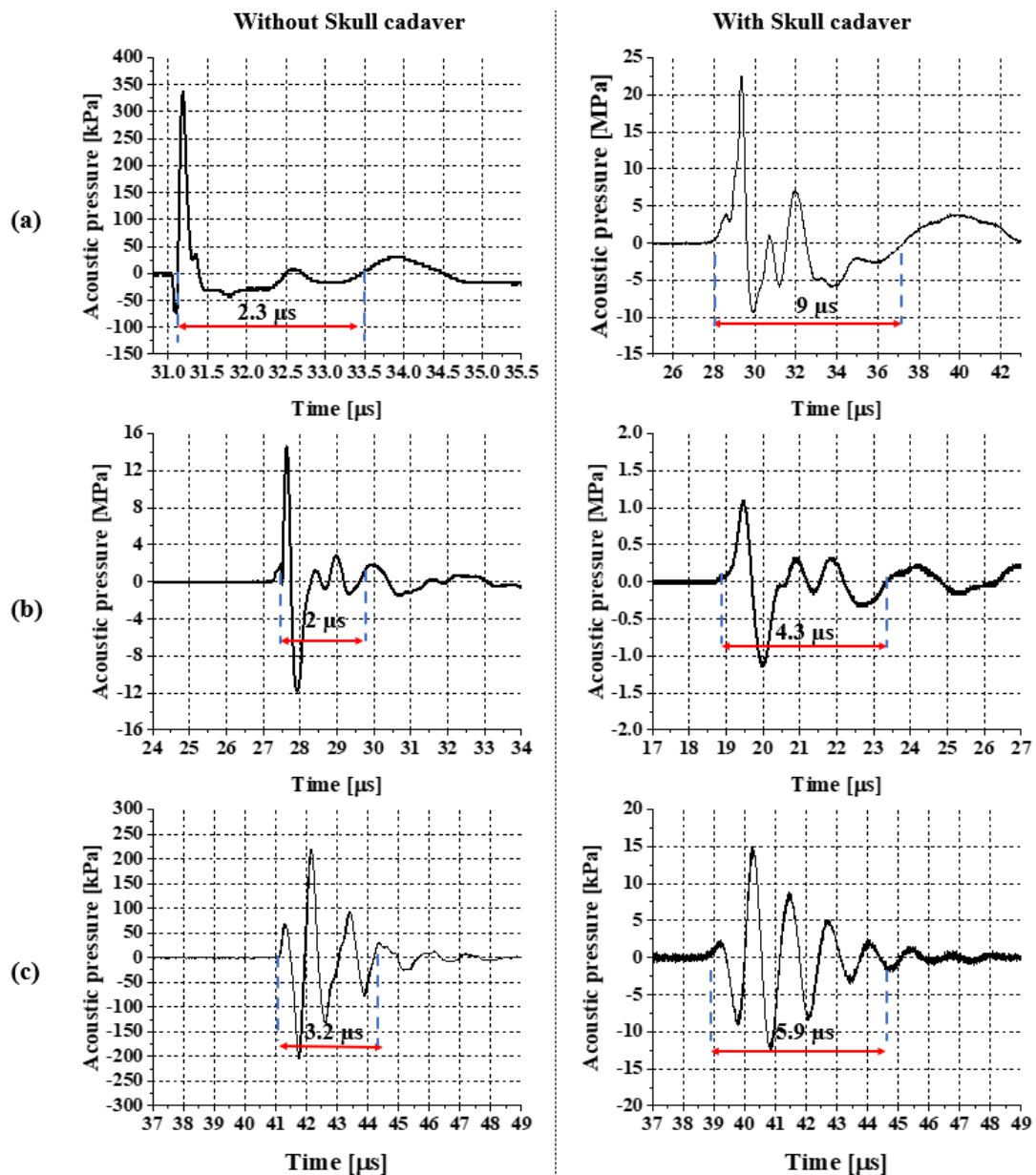


Figure 4.4 The signal generated by the CNT composite transducer before and after the penetration of LGFUS into the human skull cadaver. The signal generated by the CNT composite transducer before and after the penetration of LGFUS into the human skull cadaver, and (b) Developed CNT composite transducer. (c) The pulse wave generated by a HIFU transducer similar to the characteristics of LGFUS.

#### 4.4 Discussion

This study investigated the possibility of LGFUS generated from CNT composites penetrating human skull cadavers. We confirmed whether a very short pulse wave can penetrate a highly attenuated skull cadaver and compared how the characteristics of LGFUS change after penetration. Initially, in the absence of the skull, the LGFUS signal exhibits robust characteristics with a short rising time of 0.1  $\mu\text{s}$  and a pulse duration of 4.5  $\mu\text{s}$ , including the negative pressure. The signal's maximum positive and negative pressures are recorded at 14.6 MPa and -11.66 MPa, respectively, and the center frequency and -6 dB frequency bandwidth are 1 MHz and 2.15 MHz, respectively. However, these parameters were noticeably changed when transmitted through the skull cadaver, with reductions in maximum positive and negative pressures to 1.1 MPa and -1.1 MPa, an extension in pulse duration to 4.3  $\mu\text{s}$ , an increase in rising time to 0.78  $\mu\text{s}$ , a drop in center frequency to 464 kHz, and a reduction in -6 dB frequency bandwidth to 1.34 MHz. The comparison of signals before and after skull cadaver penetration and the signals associated with HIFU skull cadaver penetration provided valuable insights into the influence of the skull on the propagation of the LGFUS signal. Even in short pulses, the focal point was formed earlier after penetrating the skull, and it was observed that the transmission rate of LGFUS was similar to that of the HIFU signal (the shift in the focal point of LGFUS was observed, from 51.5 mm without skull cadaver penetration to 39.3 mm with skull cadaver). While the skull cadaver impacts the penetration rates of all three signals similarly, the improved CNT composite transducer exhibited the highest rate at 7.5%,

suggesting its potential for slightly better penetration rates.

The signal shape before the skull penetration of LGFUS was elongated after skull penetration, with an increased pulse duration. Additionally, the focal position of LGFUS was noted to shift forward from 50 mm to 12.4 mm after penetration, mirroring the behavior of conventional FUS (Figure 4.2 and Figure 4.3). However, it's observed that it retains a form similar to the original signal. This leads to an overall attenuation of sound pressure and loss of high frequency bands, yet the signal characteristics are well preserved. In neurostimulation studies, the sound pressure needed for brain stimulation is roughly 0.5 MPa (Kim, H. et al., 2012). Assuming that the LGFUS sound pressure is amplified either by using a higher-performance transducer than the CNT composite transducer employed in this research or by boosting the laser energy, the sound pressure post-skull penetration would increase. As this pressure rises, it's anticipated that sufficient brain stimulation could be achieved after penetrating the human skull cadaver.

The signal generated by the initial CNT composite transducer, compared to the developed CNT composite transducer, produced LGFUS with a lower output and a longer pulse duration. Two factors can account for the performance difference of LGFUS. Firstly, a substantial output difference depends on the CNT composite transducer's manufacturing method. Secondly, it's dependent on the performance of the laser system. Even when the same laser energy input from the system is applied to the transducer, the LGFUS output may vary if the laser energy per unit area received by the transducer area differs. This study prioritized investigating the

skull cadaver penetration and altering its characteristics over boosting the LGFUS output. the study was conducted to increase the output after confirming the penetration of the skull. We confirmed that high-output LGFUS generates sufficient sound pressure to stimulate the brain even after skull penetration. Furthermore, the signal generated by the HIFU transducer, with its intensity and pulse duration set similarly to LGFUS characteristics, displayed similar traits to LGFUS before and after skull penetration (Figure 4.4).

The possibility of LGFUS penetrating human skull cadavers has been confirmed. However, issues such as distortion of the focal position and reduction in output need to be addressed. CNT composite transducers can adjust the focal position and phase difference depending on the shape of the substrate lens being coated. This manufacturing flexibility allows for the design of a geometric surface that can compensate for the properties of the skull. In future work, we aim to develop a transducer with a geometric surface that can minimize focal distortion by scanning the skull and calculating the LGFUS profile needed for phase compensation.

## 4.5 Conclusion

This research demonstrated the potential for LGFUS, generated from CNT composites, to penetrate human skull cadavers, offering significant implications for future research and applications. We confirmed that a short pulse wave could successfully traverse a highly attenuated skull cadaver, and we observed a distinct transformation in LGFUS features post-penetration.

While the skull influenced the penetration rates of all signals, the developed CNT composite transducer demonstrated superior performance, suggesting its potential for better penetration rates. Despite the changes post-skull penetration, the LGFUS signal retained a similar form to the original signal, leading to an overall attenuation of sound pressure and loss of high-frequency bands, but preserving the signal characteristics.

The present research further elucidated the influence of the CNT composite transducer's fabrication process and the laser system's efficacy on the output of LGFUS. Given the results obtained, it is hypothesized that amplification in LGFUS acoustic pressure might facilitate adequate brain stimulation after penetration of the human skull cadaver. Consequently, this study not only offers pertinent knowledge regarding the impact of the skull on LGFUS signal propagation but also accentuates the prospective utility of the fabricated CNT composite transducer in forthcoming applications and investigations.

## Chapter V

### CONCLUSION AND FUTURE STUDIES

#### 5.1 Conclusion

This study expanded the application range for LGFUS from CNT composite transducers. The study elucidates the brain's response to LGFUS from optimized CNT composite transducers and shows the potential for penetration through human skull cadavers.

For the application of LGFUS generated from CNT composite transducers in research, the output of the transducers was evaluated based on the diameter and type of backing material. The performance of LGFUS was found to be superior with rigid backing, and the output changed depending on the diameter of the transducer. However, it was proven that a smaller diameter transducer can generate efficient output with the same laser energy. This contributes to technological advancements by suggesting optimal structures for efficient ultrasound generation and transducer diameters suitable for various application fields requiring ultrasound stimulation.

We stimulated rat brains using LGFUS generated by a CNT composite transducer and demonstrated that a stimulation response of EEG signals occurs when the brain is stimulated with a highly focused short-pulse ultrasound. The high spatial resolution of LGFUS allows stimulation of specific brain regions, enabling adjustment of location and depth within the

brain. This can be utilized to verify functions varying with specific locations in the brain precisely.

This research demonstrated the potential for LGFUS from CNT composites, to penetrate human skull cadavers. The study suggests that amplification in LGFUS acoustic pressure might facilitate adequate brain stimulation even after penetration through a skull cadaver. This not only offers pertinent knowledge regarding the effect of the skull on the propagation of LGFUS signals but also emphasizes the potential application of the fabricated CNT composite transducer.

In this study, we have gained important insights into the effective generation of LGFUS using CNT composite transducers and its applications in brain stimulation and precise targeting of ultrasound characteristics. This will be a foundation for new technological advancements in precise brain stimulation using FUS.

## 5.2 Future Studies

This study outlined future research in two directions. First, we've validated the intensity of LGFUS when generated by a CNT composite layer in either water or air, and we've tracked the power as a function of diameter. Based on these findings, we plan to develop an attachable CNT composite transducer. The final goal is to research and develop a portable transducer capable of generating LGFUS stimulation by attaching a CNT composite layer to the target area.

In the second, the EEG signal confirms that the response elicited by brain stimulation with LGFUS is correlated with the intensity of the LGFUS stimulation. By monitoring EEG signals in real-time during brain stimulation with LGFUS, it is possible to determine the occurrence and intensity of the stimulation. This study is limited to elucidating the relationship between the ability of LGFUS to penetrate the skull and the resulting brain stimulation by EEG monitoring. Different types of stimulation results, such as the response of actual neurons or brain cells, can occur when the brain is stimulated with LGFUS. This is closely linked to the actual ultrasound stimulation of the brain. The state of neurostimulation relies on the parameters of the ultrasound. In this study, we did not investigate the stimulation effects at the cellular or neuronal level. By evaluating ion channeling, neuronal activation, etc., when stimulating the small animal brain with LGFUS, we can propose a novel approach to identifying the mechanisms triggered by the stimulation. In addition, research is needed on precise stimulation while changing the focal point in the rat brain in the direction of the beam

and exploring different EEG responses or behavioral changes depending on the spatial resolution.

LGFUS has brought forth the potential of penetrating human skull cadavers, but the distortion of the focal spot's position and reduced output are issues that need to be addressed. CNT composite transducers can adjust the focal position and phase difference depending on the shape of the substrate lens they are coated with. This flexibility in fabrication allows for compensation by designing a geometric surface based on the properties of the skull. Therefore, in future work, we aim to develop a transducer with a geometric surface capable of minimizing the distortion of the focus by scanning the skull and calculating the required LGFUS profile for phase compensation.

## REFERENCES

- A. Ortuno (2017). "OpenBCI Github Repository," <https://github.com/OpenBCI/ultracortex> "April 24, ".
- Ashkan, K., Rogers, P., Bergman, H. and Ughratdar, I. (2017). "Insights into the mechanisms of deep brain stimulation," *Nature Reviews Neurology* **9**, 548-554.
- Aubry, J., Pauly, K. B., Moonen, C., Haar, G., Ries, M., Salomir, R., Sokka, S., Sekins, K. M., Shapira, Y. and Ye, F. (2013). "The road to clinical use of high-intensity focused ultrasound for liver cancer: technical and clinical consensus," *Journal of therapeutic ultrasound* **1**, 1-7.
- Auld, B. A. (1973). *Acoustic fields and waves in solids* (Рипол Классик).
- Baac, H. W., Lee, T. and Guo, L. J. (2013). "Micro-ultrasonic cleaving of cell clusters by laser-generated focused ultrasound and its mechanisms," *Biomedical optics express* **8**, 1442-1450.
- Baac, H. W., Ok, J. G., Lee, T. and Guo, L. J. (2015). "Nano-structural characteristics of carbon nanotube–polymer composite films for high-amplitude optoacoustic generation," *Nanoscale* **34**, 14460-14468.
- Baac, H. W., Ok, J. G., Maxwell, A., Lee, K., Chen, Y., Hart, A. J., Xu, Z., Yoon, E. and Guo, L. J. (2012). "Carbon-nanotube optoacoustic lens for focused ultrasound generation and high-precision targeted therapy," *Scientific reports*, 989.
- Baek, H., Pahk, K. J. and Kim, H. (2017). "A review of low-intensity focused ultrasound for neuromodulation," *Biomedical engineering letters*, 135-142.
- Barker, A. T., Jalinous, R. and Freeston, I. L. (1985). "Non-invasive magnetic stimulation of human motor cortex," *The Lancet* **8437**, 1106-1107.
- Beisteiner, R., Hallett, M. and Lozano, A. M. (2023). "Ultrasound Neuromodulation as a New Brain Therapy," *Advanced Science* **14**, 2205634.
- Beisteiner, R., Matt, E., Fan, C., Baldysiak, H., Schönfeld, M., Philippi Novak, T., Amini, A., Aslan, T., Reinecke, R. and Lehrner, J. (2020). "Transcranial pulse stimulation with ultrasound in Alzheimer's disease—a new navigated focal brain therapy," *Advanced Science* **3**, 1902583.
- Brighi, C., Reid, L., White, A. L., Genovesi, L. A., Kojic, M., Millar, A., Bruce, Z., Day, B. W., Rose, S. and Whittaker, A. K. (2020). "MR-guided focused ultrasound increases antibody delivery to nonenhancing high-grade glioma," *Neuro-Oncology Advances* **1**, vdaa030.

- Bronstein, J. M., Tagliati, M., Alterman, R. L., Lozano, A. M., Volkmann, J., Stefani, A., Horak, F. B., Okun, M. S., Foote, K. D. and Krack, P. (2011). "Deep brain stimulation for Parkinson disease: an expert consensus and review of key issues," *Arch. Neurol.* **2**, 165.
- Buma, T., Spisar, M. and O'Donnell, M. (2001). "High-frequency ultrasound array element using thermoelastic expansion in an elastomeric film," *Appl. Phys. Lett.* **4**, 548-550.
- Chang, W., Huang, W., Kim, J., Li, S. and Jiang, X. (2015). "Candle soot nanoparticles-polydimethylsiloxane composites for laser ultrasound transducers," *Appl. Phys. Lett.* **16**.
- Clement, G. T., Sun, J. and Hynynen, K. (2001). "The role of internal reflection in transskull phase distortion," *Ultrasonics* **2**, 109-113.
- Cleveland, R. O. and McAteer, J. A. (2012). "Physics of shock-wave lithotripsy," *Smith's textbook of endourology*, 527-558.
- Colchester, R. J., Mosse, C. A., Bhachu, D. S., Bear, J. C., Carmalt, C. J., Parkin, I. P., Treeby, B. E., Papakonstantinou, I. and Desjardins, A. E. (2014). "Laser-generated ultrasound with optical fibres using functionalised carbon nanotube composite coatings," *Appl. Phys. Lett.* **17**.
- Di, J., Kim, J., Hu, Q., Jiang, X. and Gu, Z. (2015). "Spatiotemporal drug delivery using laser-generated-focused ultrasound system," *J. Controlled Release*, 592-599.
- Drain, L. E. (2019). *Laser ultrasonics techniques and applications* (Routledge).
- Foley, J. L., Little, J. W. and Vaezy, S. (2007). "Image-guided high-intensity focused ultrasound for conduction block of peripheral nerves," *Ann. Biomed. Eng.*, 109-119.
- Fregni, F. and Pascual-Leone, A. (2007). "Technology insight: noninvasive brain stimulation in neurology—perspectives on the therapeutic potential of rTMS and tDCS," *Nature clinical practice Neurology* **7**, 383-393.
- Frehlick, Z., Lakhani, B., Fickling, S. D., Livingstone, A. C., Danilov, Y., Sackier, J. M. and D'Arcy, R. C. (2019). "Human translingual neurostimulation alters resting brain activity in high-density EEG," *Journal of neuroengineering and rehabilitation* **1**, 1-7.
- Fry, F. J. (1977). "Transkull transmission of an intense focused ultrasonic beam," *Ultrasound in Medicine and Biology* **2**, 183-184.
- Fry, F. J., Ades, H. W. and Fry, W. J. (1958). "Production of reversible changes in the central nervous system by ultrasound," *Science* **3289**, 83-84.
- George, M. S. and Aston-Jones, G. (2010). "Noninvasive techniques for probing neurocircuitry and treating illness: vagus nerve stimulation (VNS), transcranial magnetic stimulation (TMS) and transcranial direct current stimulation (tDCS)," *Neuropsychopharmacology* **1**, 301-316.

Gisuk Kim, Moojoon Kim, Kanglyeol Ha, Jooho Lee, Dong-Guk Paeng and Min Joo Choi (2019). "Waveform characteristics of ultrasonic wave generated from CNT/PDMS composite," *The Journal of the Acoustical Society of Korea* **4**, 459-466.

Gwan-Suk Kang (2018). "Acoustic and Optical Characteristics of Cavitation Bubble Clouds Produced by Shock Wave Pulse,".

Heo, J., Biswas, D., Park, K. K., Son, D., Park, H. J. and Baac, H. W. (2021). "Laser-generated focused ultrasound transducer using a perforated photoacoustic lens for tissue characterization," *Biomedical optics express* **3**, 1375-1390.

Horvath, J. C., Forte, J. D. and Carter, O. (2015). "Evidence that transcranial direct current stimulation (tDCS) generates little-to-no reliable neurophysiologic effect beyond MEP amplitude modulation in healthy human subjects: a systematic review," *Neuropsychologia*, 213-236.

Hsieh, B., Kim, J., Zhu, J., Li, S., Zhang, X. and Jiang, X. (2015). "A laser ultrasound transducer using carbon nanofibers–polydimethylsiloxane composite thin film," *Appl. Phys. Lett.* **2**.

Hynynen, K. and Jolesz, F. A. (1998). "Demonstration of potential noninvasive ultrasound brain therapy through an intact skull," *Ultrasound Med. Biol.* **2**, 275-283.

Hynynen, K., McDannold, N., Clement, G., Jolesz, F. A., Zadicario, E., Killiany, R., Moore, T. and Rosen, D. (2006). "Pre-clinical testing of a phased array ultrasound system for MRI-guided noninvasive surgery of the brain—a primate study," *Eur. J. Radiol.* **2**, 149-156.

Jagannathan, J., Sanghvi, N. K., Crum, L. A., Yen, C., Medel, R., Dumont, A. S., Sheehan, J. P., Steiner, L., Jolesz, F. and Kassell, N. F. (2009). "High intensity focused ultrasound surgery (HIFU) of the brain: A historical perspective, with modern applications," *Neurosurgery* **2**, 201.

Jasper, H. H. (1958). "The ten-twenty electrode system of the International Federation," *Electroencephalogr.Clin.Neurophysiol.*, 370-375.

Jiricek, S., Koudelka, V., Lacik, J., Vejmla, C., Kuratko, D., Wójcik, D. K., Raida, Z., Hlinka, J. and Palenicek, T. (2021). "Electrical source imaging in freely moving rats: Evaluation of a 12-electrode cortical electroencephalography system," *Frontiers in neuroinformatics*, 589228.

Kalia, S. K., Sankar, T. and Lozano, A. M. (2013). "Deep brain stimulation for Parkinson's disease and other movement disorders," *Curr. Opin. Neurol.* **4**, 374-380.

Khokhlova, T. D., Haider, Y. A., Maxwell, A. D., Kreider, W., Bailey, M. R. and Khokhlova, V. A. (2017). "Dependence of boiling histotripsy treatment efficiency on HIFU frequency and focal pressure levels," *Ultrasound Med. Biol.* **9**, 1975-1985.

Kim, H., Chiu, A., Lee, S. D., Fischer, K. and Yoo, S. (2014). "Focused ultrasound-mediated non-invasive brain stimulation: examination of sonication parameters," *Brain stimulation* **5**, 748-756.

- Kim, H., Taghados, S. J., Fischer, K., Maeng, L., Park, S. and Yoo, S. (2012). "Noninvasive transcranial stimulation of rat abducens nerve by focused ultrasound," *Ultrasound Med. Biol.* **9**, 1568-1575.
- Kim, J., Chang, W., Lindsey, B. D., Dayton, P. A., Dai, X., Stavas, J. M. and Jiang, X. (2016). "Laser-generated-focused ultrasound transducers for microbubble-mediated, dual-excitation sonothrombolysis," 1-4.
- King, R. L., Brown, J. R., Newsome, W. T. and Pauly, K. B. (2013). "Effective parameters for ultrasound-induced in vivo neurostimulation," *Ultrasound Med. Biol.* **2**, 312-331.
- Kobayashi, M. and Pascual-Leone, A. (2003). "Transcranial magnetic stimulation in neurology," *The Lancet Neurology* **3**, 145-156.
- Krishna, V., Sammartino, F. and Rezai, A. (2018). "A review of the current therapies, challenges, and future directions of transcranial focused ultrasound technology: advances in diagnosis and treatment," *JAMA neurology* **2**, 246-254.
- Kubaneck, J., Shukla, P., Das, A., Baccus, S. A. and Goodman, M. B. (2018). "Ultrasound elicits behavioral responses through mechanical effects on neurons and ion channels in a simple nervous system," *Journal of Neuroscience* **12**, 3081-3091.
- Kung, Y., Lan, C., Hsiao, M., Sun, M., Hsu, Y., Huang, A. P., Liao, W., Liu, H., Inserra, C. and Chen, W. (2018). "Focused shockwave induced blood-brain barrier opening and transfection," *Scientific reports* **1**, 1-11.
- Lee, T., Baac, H. W., Li, Q. and Guo, L. J. (2018). "Efficient photoacoustic conversion in optical nanomaterials and composites," *Advanced Optical Materials* **24**, 1800491.
- Lee, W., Chung, Y. A., Jung, Y., Song, I. and Yoo, S. (2016). "Simultaneous acoustic stimulation of human primary and secondary somatosensory cortices using transcranial focused ultrasound," *BMC neuroscience* **1**, 1-11.
- Leksell, L. (1956). "Echo-encephalography. 1. Detection of intracranial complications following brain injury," *Acta Chir. Scand.*, 301-315.
- Li, J., Lan, X., Lei, S., Ou-Yang, J., Yang, X. and Zhu, B. (2019). "Effects of carbon nanotube thermal conductivity on optoacoustic transducer performance," *Carbon*, 112-118.
- Li, Y., Song, A., Qiu, W., Gong, S., Wu, D., Xiao, Z., Jiang, Y. and Zhu, Z. (2019). "Electrical characterization of flexible CNT/polydimethylsiloxane composite films with finite thickness," *Carbon*, 439-447.
- Lin, K., Kim, Y., Maxwell, A. D., Wang, T., Hall, T. L., Xu, Z., Fowlkes, J. B. and Cain, C. A. (2014). "Histotripsy beyond the intrinsic cavitation threshold using very short ultrasound pulses: microtripsy," *IEEE Trans. Ultrason. Ferroelectr. Freq. Control* **2**, 251-265.

- Lingeman, J. E., McAteer, J. A., Gnessin, E. and Evan, A. P. (2009). "Shock wave lithotripsy: advances in technology and technique," *Nature Reviews Urology* **12**, 660-670.
- Loo, C. K. and Mitchell, P. B. (2005). "A review of the efficacy of transcranial magnetic stimulation (TMS) treatment for depression, and current and future strategies to optimize efficacy," *J. Affect. Disord.* **3**, 255-267.
- McDannold, N., Vykhodtseva, N., Raymond, S., Jolesz, F. A. and Hynynen, K. (2005). "MRI-guided targeted blood-brain barrier disruption with focused ultrasound: histological findings in rabbits," *Ultrasound Med. Biol.* **11**, 1527-1537.
- Meyers, R., Fry, W. J., Fry, F. J., Dreyer, L. L., Schultz, D. F. and Noyes, R. F. (1959). "Early experiences with ultrasonic irradiation of the pallidofugal and nigral complexes in hyperkinetic and hypertonic disorders," *J. Neurosurg.* **1**, 32-54.
- Miranda, I., Souza, A., Sousa, P., Ribeiro, J., Castanheira, E. M., Lima, R. and Minas, G. (2021). "Properties and applications of PDMS for biomedical engineering: A review," *Journal of functional biomaterials* **1**, 2.
- Moon, C., Fan, X., Ha, K. and Kim, D. (2017). "Generation of planar blast waves using carbon nanotubes-poly-dimethylsiloxane optoacoustic transducer," *AIP Advances* **1**, 015107.
- Nelson, E., Lindstrom, P. A. and Haymaker, W. (1959). "Pathological effects of ultrasound on the human brain: a study of 25 cases in which ultrasonic irradiation was used as a lobotomy procedure," *Journal of Neuropathology & Experimental Neurology* **4**, 489-508.
- Nitsche, M. A. and Paulus, W. (2000). "Excitability changes induced in the human motor cortex by weak transcranial direct current stimulation," *J. Physiol. (Lond.)* **Pt 3**, 633.
- Pernot, M., Aubry, J., Tanter, M., Andre, F. and Fink, M. (2004). "Prediction of the skull overheating during high intensity focused ultrasound transcranial brain therapy," 1005-1008.
- Pichardo, S. and Hynynen, K. (2007). "Treatment of near-skull brain tissue with a focused device using shear-mode conversion: a numerical study," *Physics in Medicine & Biology* **24**, 7313.
- Pinton, G., Aubry, J., Bossy, E., Muller, M., Pernot, M. and Tanter, M. (2012). "Attenuation, scattering, and absorption of ultrasound in the skull bone," *Med. Phys.* **1**, 299-307.
- Plaksin, M., Kimmel, E. and Shoham, S. (2016). "Cell-type-selective effects of intramembrane cavitation as a unifying theoretical framework for ultrasonic neuromodulation," *eneuro* **3**.
- Ram, Z., Cohen, Z. R., Harnof, S., Tal, S., Faibel, M., Nass, D., Maier, S. E., Hadani, M. and Mardor, Y. (2006). "Magnetic resonance imaging-guided, high-intensity focused ultrasound for brain tumor therapy," *Neurosurgery* **5**, 949-956.
- Shi, H., Ok, J. G., Won Baac, H. and Jay Guo, L. (2011). "Low density carbon nanotube forest as an index-matched and near perfect absorption coating," *Appl. Phys. Lett.* **21**.

- Tanter, M., Thomas, J. and Fink, M. (1998). "Focusing and steering through absorbing and aberrating layers: Application to ultrasonic propagation through the skull," *J. Acoust. Soc. Am.* **5**, 2403-2410.
- Tempny, C. M., McDannold, N. J., Hynynen, K. and Jolesz, F. A. (2011). "Focused ultrasound surgery in oncology: overview and principles," *Radiology* **1**, 39-56.
- Theodore, W. H. and Fisher, R. (2007). "Brain stimulation for epilepsy," *Operative Neuromodulation: Volume 2: Neural Networks Surgery*, 261-272.
- Tobias, J., Hynynen, K., Roemer, R., Guthkelch, A. N., Fleischer, A. S. and Shively, J. (1987). "An ultrasound window to perform scanned, focused ultrasound hyperthermia treatments of brain tumors," *Med. Phys.* **2**, 228-234.
- Tong, L. H., Lim, C. W. and Li, Y. C. (2014). "Generation of high-intensity focused ultrasound by carbon nanotube opto-acoustic lens," *Journal of Applied Mechanics* **8**, 081014.
- Tsui, P., Wang, S. and Huang, C. (2005). "In vitro effects of ultrasound with different energies on the conduction properties of neural tissue," *Ultrasonics* **7**, 560-565.
- Tufail, Y., Matyushov, A., Baldwin, N., Tauchmann, M. L., Georges, J., Yoshihiro, A., Tillery, S. I. H. and Tyler, W. J. (2010). "Transcranial pulsed ultrasound stimulates intact brain circuits," *Neuron* **5**, 681-694.
- Tyler, W. J., Tufail, Y., Finsterwald, M., Tauchmann, M. L., Olson, E. J. and Majestic, C. (2008). "Remote excitation of neuronal circuits using low-intensity, low-frequency ultrasound," *PloS one* **10**, e3511.
- Van Lier, H., Drinkenburg, W. H., Van Eeten, Y. J. and Coenen, A. M. (2004). "Effects of diazepam and zolpidem on EEG beta frequencies are behavior-specific in rats," *Neuropharmacology* **2**, 163-174.
- Vyazovskiy, V. V. and Tobler, I. (2005). "Theta activity in the waking EEG is a marker of sleep propensity in the rat," *Brain Res.* **1-2**, 64-71.
- Wetsel, G. C. (1986). "Photothermal generation of thermoelastic waves in composite media," *IEEE Trans. Ultrason. Ferroelectr. Freq. Control* **5**, 450-461.
- White, D. N., Clark, J. M., Chesebrough, J. N., White, M. N. and Campbell, J. K. (1968). "Effect of the skull in degrading the display of echoencephalographic B and C scans," *J. Acoust. Soc. Am.* **5**, 1339-1345.
- Won Baac, H., Ok, J. G., Park, H. J., Ling, T., Chen, S., Hart, A. J. and Guo, L. J. (2010). "Carbon nanotube composite optoacoustic transmitters for strong and high frequency ultrasound generation," *Appl. Phys. Lett.* **23**.

Xu, Z., Hall, T. L., Vlaisavljevich, E. and Lee Jr, F. T. (2021). "Histotripsy: the first noninvasive, non-ionizing, non-thermal ablation technique based on ultrasound," *International Journal of Hyperthermia* **1**, 561-575.

Ye, P. P., Brown, J. R. and Pauly, K. B. (2016). "Frequency dependence of ultrasound neurostimulation in the mouse brain," *Ultrasound Med. Biol.* **7**, 1512-1530.

Yoo, S., Bystritsky, A., Lee, J., Zhang, Y., Fischer, K., Min, B., McDannold, N. J., Pascual-Leone, A. and Jolesz, F. A. (2011). "Focused ultrasound modulates region-specific brain activity," *Neuroimage* **3**, 1267-1275.

## ACKNOWLEDGEMENTS

길다면 길고 짧다면 짧은 7 년동안 제주대학교 대학원의 석, 박사 과정을 하면서 많은 분들의 도움을 받으면서 마치게 되었습니다. 박사 학위 논문을 마무리하면서 도움과 배려를 해주신 모든 분들께 감사의 인사를 드립니다.

먼저, 독립적인 연구자가 되어야 한다고 항상 말씀하시던 팽동국 교수님의 연구자의 태도와 방향에 대한 조언 등을 통해 진정한 연구자의 길로 첫 발을 내딛을 수 있었음에 감사드립니다. 그리고 바쁘신 와중에 본 논문의 심사를 해주셨던 박진형 교수님, 강윤정 교수님, 유보경 교수님께 감사드립니다. 대학원 생활동안 연구 내용에 대한 조언을 통해 직, 간접적으로 도움을 주셨던 조일형 교수님, 이종현 교수님, 배진호 교수님께 감사드립니다. 연구실에서 함께 알가알부하며 힘들 때나 즐거울 때 항상 함께하였던 민수홍, 이청아, 정인용, 임승욱, 고준빈에게 감사하며, 짧지만 한 연구실에서 같이 생활한 이기배, 김정민, 고건혁, 박흥진, 고영빈과 행적적으로 수월하게 서류 절차를 진행할 수 있게 도움을 준 김수경, 양인재 조교에게 감사의 마음을 전합니다.

마지막으로, 항상걱정과 위로를 해주시며 어떤 결정을 선택하든 항상 이해해주시고 응원해주셨던 저의 부모님께 감사드립니다. 여러가지 고민이 있을 때마다 조언을 아끼지 않은 형에게 감사의 마음을 전하며, 부족하지만 최선을 다한 이 논문을 가족에게 바칩니다.